KeAi

CHINESE ROOTS
GLOBAL IMPACT

Contents lists available at ScienceDirect

Petroleum Science

journal homepage: www.keaipublishing.com/en/journals/petroleum-science



Original Paper

Enhancing shale oil recovery with water-alternating-CO₂ injection through radial borehole fracturing



Jia-Cheng Dai ^a, Tian-Yu Wang ^{b, *}, Ye Zhang ^{c, d, **}, Zhi-Ping Zhang ^{c, d}, Chun-Lin Zeng ^{c, d}, Kang-Jian Tian ^b, Jing-Bin Li ^b, Shou-Ceng Tian ^b, Gen-Sheng Li ^b

- ^a Karamay Branch of State Key Laboratory of Petroleum Resources and Engineering, China University of Petroleum-Beijing at Karamay, Karamay, 834000, Xinjiang, China
- ^b State Key Laboratory of Petroleum Resources and Engineering, China University of Petroleum (Beijing), Beijing, 102249, China
- c Key Laboratory of Shale Gas Exploration, Ministry of Natural Resources (Chongqing Institute of Geology and Mineral Resources), Chongqing, 401120, China
- ^d National and Local Joint Engineering Research Center of Shale Gas Exploration and Development (Chongqing Institute of Geology and Mineral Resources), Chongqing, 401120, China

ARTICLE INFO

Article history: Received 29 October 2024 Received in revised form 15 April 2025 Accepted 22 April 2025 Available online 23 April 2025

Edited by Yan-Hua Sun

Keywords:
Horizontal well fracturing
Enhanced shale oil recovery
Radial borehole fracturing
Water-alternating-gas
Numerical reservoir model

ABSTRACT

This paper introduces a novel approach combining radial borehole fracturing with Water-Alternating-Gas (WAG) injection, enabling simultaneous WAG injection and shale oil production in a single vertical well. A numerical reservoir model incorporating the modified exponential non-Darcy law, stress sensitivity, and diffusion is established. The spatial distribution of permeability reduction shows that stress sensitivity enhances the non-Darcy effect, with apparent permeability decreasing to 0–92.1% of the initial value, highlighting the importance of maintaining reservoir pressure. Continuous CO₂ flooding leads to early gas breakthrough, while continuous water flooding has less displacement efficiency. A 30% water-to-gas injection time ratio improves oil production and delays gas breakthrough compared to continuous CO₂ injection. Optimal conditions for effective recovery are identified as an initial production period of 100 d and a well vertical spacing of 30 m. This study compares the production capacity of WAG operations under radial borehole fracturing and horizontal well fracturing. When the number of wells is two for both cases, the production capacity of radial borehole fracturing is comparable to that of five-stage horizontal well fracturing, indicating that radial borehole fracturing can serve as an alternative or supplement to horizontal well fracturing when the reservoir volume is limited. This study offers a new method and theoretical basis for the efficient development of shale oil.

© 2025 The Authors. Publishing services by Elsevier B.V. on behalf of KeAi Communications Co. Ltd. This is an open access article under the CC BY license (http://creativecommons.org/licenses/by/4.0/).

1. Introduction

Regarded as an unconventional hydrocarbon resource, shale oil is confined within organically-rich shale formations, representing an estimated 20%–50% of the global crude oil reserves (Caineng et al., 2013). The distinctive characteristics of shale oil include ultra-low permeability, ranging from nano-Darcy to milli-Darcy, along with the presence of nano- and micro-pores (Shen and Sheng, 2018; Xia et al., 2021). Therefore, the employment of reservoir simulation approaches that integrate horizontal wells

Peer review under the responsibility of China University of Petroleum (Beijing).

with hydraulic fracturing is recognized as an effective mechanism for creating a Stimulated Reservoir Volume (SRV), intended to enhance the reservoir permeability (Deng et al., 2022; Suliman et al., 2013). Radial boreholes influences fracture orientation, and can create multi-layer fractures (Guo et al., 2017; Dai et al., 2023a). However, the initial production rate often undergoes a reduction to roughly 10%–20% within the first few years of the depletion production, leaving a substantial 75%–95% of the initial oil in place (Altawati et al., 2021). Water flooding is preferred due to its simplicity, cost-effectiveness, and effectiveness in conventional reservoirs. However, applying water flooding in shale oil reservoirs faces challenge of inability of water to effectively mobilize residual oil (Afari et al., 2022). Therefore, the application of enhanced oil recovery (EOR) methods to maintain reservoir pressure, displace residual oil and promote shale oil production proves indispensable.

The injection of carbon dioxide (CO₂) is gaining recognition for

st Corresponding author.

^{**} Corresponding author.

E-mail addresses: wangty@cup.edu.cn (T.-Y. Wang), zhangye_sg@vip.163.com Y Zhang)

its EOR capacity (Khurshid and Afgan, 2021a). As one of the technological foundations for Carbon Capture, Utilization, and Storage (CCUS), CO₂-EOR is spearheading efforts to sequester captured CO₂ in oilfields across the United States. Approximately 68 million tons of CO₂ from natural and industrial sources were transported to EOR sites in 2015 (Callahan et al., 2014). On a microscopic scale, CO₂ molecules possess pronounced diffusion properties, allowing them to migrate to locations beyond the reach of water (Jia et al., 2019b: Zhao et al., 2020). Moreover, CO₂ can effectively replace part of the adsorbed hydrocarbon molecules via competitive adsorption (Liu et al., 2017). CO₂ generally exists in a supercritical state under subsurface conditions. Sc-CO₂ efficiently extracts light hydrocarbon components from oil (Li et al., 2019), and extensively dissolves into oil (Tovar et al., 2021), leading oil swelling, viscosity reduction, alteration of oil—water interfacial tension, and liberation of trapped oil (Li et al., 2013; Wang et al., 2022; Zhu et al., 2018). On a microscopic scale, when the pressure exceeds the minimum miscibility pressure, the CO₂-oil interface disappears, giving rise to a piston-like front (Stalkup, 1978; Guo Y. et al., 2022). However, the high mobility of CO₂ can easily meet the challenge of gas early breakthrough (Gao et al., 2014), bypassing regions with low permeability (Massarweh and Abushaikha, 2022). Consequently, this poor sweep efficiency can diminish overall oil recovery and lead to CO₂ wastage, especially in a continuous CO₂ flooding (CI) case.

Considering the challenges of CI, Water-Alternating-Gas (WAG) injection emerges as a promising solution (Khurshid and Afgan, 2021b, 2022). WAG achieves a more stable displacement front and mitigates CO₂ breakthrough problems by reducing the mobility ratio between the injectant and the oil (Afzali et al., 2018). The water phase enhances sweep efficiency by obstructing high permeability channels, thereby facilitating and directing the subsequent injection of CO₂ (Wang et al., 2020). Additionally, water helps control the reservoir pressure and reduce CO₂ requirements (Chen et al., 2010). An average increase in oil recovery of up to 10% of the original oil in place is found in previous study (Skauge and Stensen, 2003; Afzali et al., 2018). For a nine-injection well scenario proposed by Ren et al. (2023), WAG increases oil production by 16.2% and reduce CO₂ consumption by 15%.

Numerous projects proves that the WAG technique caneffectually enhance oil recovery (Khurshid et al., 2022a, 2022b; Sun et al., 2021), with example from Norwegian WAG project accomplishing an ultimate recovery factor between 53% and 66% (Tovar et al., 2021; Hinderaker and Njaa, 2010). However, within homogenous and significantly thick conventional reservoirs, water and gas articulate a discernible separation. The disparate densities of water and gas further amplify gravitational segregation during the displacement, subsequently diminishing the efficiency of the displacement (Faisal et al., 2009; Claridge, 1982). Due to the imperative of large-scale hydraulic fracturing for the development of unconventional reservoirs (Orangi et al., 2011; Wan and Sheng, 2015), the direct application of continuous gas driving has been prone to gas breakthrough; consequently, WAG is considered (Ghaderi et al., 2012a).

This study presents a new solution to gravitational segregation challenges by an integrated WAG method coupled with radial borehole fracturing, as shown in Fig. 1. In a single vertical or inclined well, the radial borehole fracturing-WAG method involves creating hydraulic fractures in both upper and lower layers using radial boreholes, with one layer serving as the production well and the other as the WAG injection well. This approach alters the flow direction vertically, distinguishing it from traditional WAG methods, thus avoiding gravitational segregation and reducing drilling costs (Bruni et al., 2007; Ragab and Kamel, 2013; Maut et al., 2017; Dai et al., 2023b).

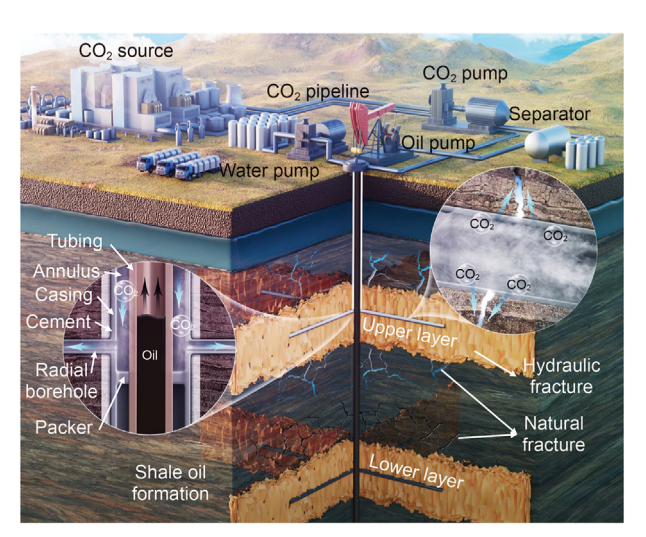


Fig. 1. Schematic diagram of the radial borehole fracturing-WAG process (In the natural fractures, blue represents water, white represents CO₂, and black represents shale oil)

The geological settings considered in WAG studies have progressed from homogeneous idealized formations to more complex configurations, such as heterogeneous, fractured, and multi-layered reservoirs (Khan and Mandal, 2022a). Previous study builds WAG numerical models, incorporating the effects of multiphase permeability characteristics (capillary pressure and hysteresis effects) and phase behavior characteristics (immiscible, miscible, and nearmiscible) (Afzali et al., 2020). WAG injection has also been considered for application in CO₂ storage in saline aguifers. Based on multiphase flow dynamics, the modeling framework has been further coupled with heat transfer and chemical reactions (Awolayo et al., 2025; Wang et al., 2023). In recent years, artificial intelligent models integrated with numerical methods for WAG production are built. For example, Qi et al. (2024) utilized an XGBoost model in conjunction with a hybrid genetic algorithm to predict oil recovery and carbon storage efficiency. Based on the LSTM neural network approach, Asante et al. (2024) developed a predictive model for oil production under CO₂ WAG injection. The model incorporated parameters including pressures, WAG cycles, and injection volumes to predict oil recovery.

WAG injection is considered advantageous for mitigating the issues of early-breakthrough caused by uneven fracture distribution and heterogeneity in shale oil reservoirs. However, the unique mechanisms of shale oil reservoirs, such as complex fracture networks and strong matrix-fracture interactions, necessitate adjustments to the conventional WAG flow simulation approaches used in conventional reservoirs (Yang et al., 2022; Afzali et al., 2018; Khan and Mandal, 2022b). In the SRV formed post-fracturing, stress sensitivity is a key effect affecting fluid flowing through the matrix and fractures (Xiao et al., 2016). Changes in effective stress can induce alterations in fracture width, potentially causing fracture closure and significantly impacting fluid conductivity (Yang D. et al., 2019). Therefore, Gangi (1978) developed a model using a conceptual bed of nails to account for changes in fracture permeability due to pressure and confining stress. The non-Darcy flow is another effect that is commonly encountered in the shale oil reservoir. When non-Darcy flow is significant, the relation between pressure differential and fluid velocity demonstrates a deviation from the linear relationship typically described by Darcy's law, particularly at lower pressure differentials (Yao and Ge, 2011). This non-linearity can be attributed to fluid inertia, fluid slippage at the rock surface, or altered flow paths (Zeng et al., 2010).

J.-C. Dai, T.-Y. Wang, Y. Zhang et al. Petroleum Science 22 (2025) 2950–2966

While previous studies generally demonstrate the impact of the stress sensitivity and non-Darcy effect on the final recovery rate (Wang et al., 2017). For example, Zhao et al. (2023) observed that stress sensitivity-induced reductions in hydraulic fracture permeability can lead to a 5% decrease in cumulative gas production over a decade. Meanwhile, Wang and Sheng (2017) indicated that the ultimate oil recovery factor under non-Darcy flow approximates 80% of that under Darcy flow. Moreover, according to Wang and Sheng's model, non-Darcy behavior correlates with apparent permeability and viscosity. It demonstrates that the variation of permeability under stress sensitivity affects non-Darcy flow behavior. Therefore, investigating the coupling relationship between these two phenomena provides guidance for accurately understanding the fluid flow in shale oil reservoirs. Wu et al. (2021) have experimentally measured the data on critical pressure gradient and stress sensitivity in WAG injection. A model coupling non-Darcy flow and stress sensitivity in shale oil reservoirs can provide valuable references for WAG applications. Table 1 summarizes representative studies considering the effects of non-Darcy flow and stress sensitivity. Non-Darcy models are exemplified by the boundary-layer effect model, the threshold pressure gradient (TPG) linear model, and the exponential model, while stress sensitivity models are represented by the exponential model and the Gangi model. It is currently widely acknowledged that stress sensitivity can enhance the non-Darcy effect. However, the spatial distribution analysis of the coupled effects of these two phenomena remains inadequate.

This study builds a new flow model integrating stress sensitivity. non-Darcy effects, and diffusion. A coupling mechanism between stress sensitivity and non-Darcy effects is considered. The issue of negative formula factors in the Wang and Sheng's model under low mobility conditions is addressed and corrected, thereby enhancing the model's applicability. The spatial distribution characteristics of the coupled effects of stress sensitivity and non-Darcy effects are also presented for the first time. This provides insights into identifying hard-to-mobilize regions in the reservoir caused by non-Darcy flow and stress sensitivity, and offers a basis for adjusting production strategies. Moreover, the effects of operating and drilling parameters, including water-to-gas injection time ratio, primary production time, and layer spacing, are investigated in this study, presenting an innovative approach and its theoretical foundation to enhance the cost-effective development of shale oil resources.

2. Methodology

2.1. Radial borehole fracturing-WAG method

A method of WAG combined with radial borehole fracturing is proposed. As shown in Fig. 2, a vertical main well is drilled from the surface to the target shale reservoir and cemented with a casing. Using a hydraulic drill bit, four radial boreholes are drilled in the upper and lower layers of the main well, followed by hydraulic fracturing. These radial boreholes, with radii generally ranging from 20 to 50 mm, extend outward from the main well to lengths between 10 and 100 m (Liu et al., 2018). The radial boreholes affect hydraulic fractures propagate direction (Guo Z. et al., 2022). After hydraulic fracturing, tubing is lowered into the wellbore, and isolating packers are placed between the upper and lower radial boreholes. This design allows for two operational modes: depletion production and WAG. In the former, both upper and lower radial

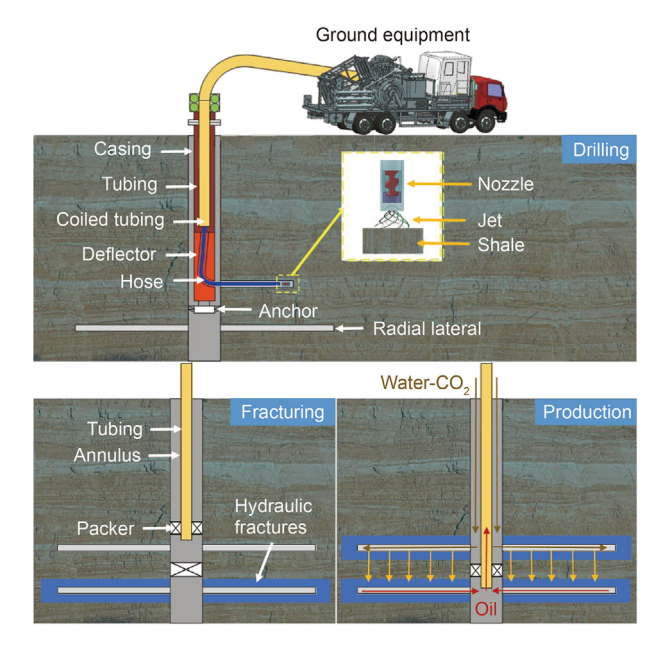


Fig. 2. Schematic illustration of the drilling, fracturing, and WAG processes in a radial well.

Table 1Non-Darcy and stress sensitivity model review.

Scale and porous media	Non-Darcy coefficient	Stress sensitivity coefficient	Remarks	References
Core flooding experiment and simulation on Qianjiang shale rock	$\left(1 - \frac{h}{r_{\rm ori}}\right)^4$	$\frac{\mathrm{e}^{-ab}(1-\mathrm{e}^{-a\Delta P})}{a\Delta P}$	The linear flow portion of the seepage flow curve is dependent upon the combined effects of stress sensitivity and the boundary layer.	Lei et al. (2019)
Analytical model of multistage fractured horizontal wells	TPG	$\mathrm{e}^{\gamma\Delta P}$	The study analyzed the effects of critical pressure gradient, permeability modulus, and fracture density on the dimensionless pressure derivative.	Wu et al. (2019)
Core flooding experiment on artificial cores	TPG	$0.974e^{-0.013P_d}$	Stress sensitivity would intensify the influence of pseudo-TPG, which results in a much lower production rate and recovery factor.	Dong et al. (2019)
Core flooding experiment on Nantun sandstone	Three-section TPG non-Darcy seepage model	$\left(\frac{\phi}{\phi_0}\right)^{lpha}$	Reservoirs with high stress sensitivity have large starting pressure gradients.	Liu B. et al. (2020)
Analytical model of flowing in bundle of tortuous capillary tubes	TPG and nonflowing liquid boundary layer	$\mathrm{e}^{\gamma\Delta P}$	(1) When the pore compressibility is positive, the apparent liquid permeability <i>K</i> increases with increasing pressure gradient.(2) The TPG for the oil phase increases with the increase in effective stress.	Cheng et al. (2023); Qu et al. (2024)
Numerical model of flowing in bundle of tortuous capillary tubes	$\frac{1}{1 + a\mathrm{e}^{-b \nabla P }}$	$\left[1-\left(\frac{\sigma_{\rm C}-\alpha_{\rm B}P}{\sigma_{\rm 1}}\right)^m\right]^3$	stress. ${\rm CO_2}$ huff-n-puff mitigates adverse effects of non-Darcy and stress sensitivity effect on production performance.	Rui et al. (2025)

boreholes serve as production wells, with the oil produced from the radial boreholes and flowing to surface through tubing and annulus. In the latter, at the surface, the annulus is connected to a water pump and a CO_2 injection pump. Water and CO_2 gas are alternately injected into the subsurface through the annulus. The upper radial boreholes act as the WAG injection layer, displacing oil downward to the lower radial boreholes.

Radial borehole fracturing-WAG method can utilize multi-layer fractures to enhance reservoir utilization and reduce the cost of well drilling. The same radial borehole fracturing configuration can also be applied to scenarios such as water flooding, continuous CO₂ injection, and CO₂ huff-n-puff (Dai et al., 2023b, 2023c, 2023d). In order to characterize the downhole fluid flow of the method and predict the oil production and CO₂ storage of the WAG method, the following numerical simulation method is established.

2.2. Model assumptions

A compositional model affords a more accurate portrayal of the multiphase and multicomponent dynamics during the WAG process (Tian et al., 2019). To optimize simulation convergence, several assumptions are made: The reservoir temperature remains isothermal, unaffected by the injection of $\rm CO_2$; $\rm CO_2$ sorption and dissolution in water, capillary pressure, hysteresis in relative permeability, nano-pore confinement effects, and impacts of asphaltenes and hydration formation are ignored.

2.3. Compositional mode formulation

For the oil and gas phases, the mass conservation equation for the matrix considering molecular diffusion can be expressed as follows:

$$\partial_{t} \left[\phi \sum_{\alpha = \mathbf{o}, \mathbf{g}} \rho_{\alpha} S_{\alpha} X_{\alpha}^{i} \right] + \sum_{\alpha = \mathbf{o}, \mathbf{g}} \nabla \cdot \left(\rho_{\alpha} X_{\alpha}^{i} \boldsymbol{v}_{\alpha} + J_{\alpha}^{i} \right) - \sum_{\alpha = \mathbf{o}, \mathbf{g}} \rho_{\alpha} X_{\alpha}^{i} q_{\alpha} / V = 0$$

$$\tag{1}$$

where J_{α}^{i} represents the diffusive mass flux of component i in phase α , m^{2}/s . It is written as follows:

$$J_{\alpha}^{i} = -\frac{\phi S_{\alpha}}{\tau_{\alpha}} D_{\alpha}^{i} \nabla \left(r_{\alpha} X_{\alpha}^{i} \right) \tag{2}$$

For the water phase, generally ignoring the diffusion effect, the mass conservation equation is

$$\partial_t [\phi \rho_w S_w] + \nabla \cdot (\rho_w \mathbf{v}_w) - \rho_w q_w / V = 0 \tag{3}$$

where ϕ represents the porosity of the matrix; ρ represents phase density, kg/m³; S represents phase saturation; X represents the mass fraction; Y is the Darcy velocity, m/s; Y is the volumetric flow rate, m³/s; Y is the volume of the cell, m³; Y represents the diffusion coefficient of component Y in phase Y is the tortuosity; subscripts w, o, and g denote the water, liquid, and gas hydrocarbon phases correspondingly. The division of volumetric flow rates (Y by volume Y ensures dimensional consistency across all terms in the equation.

When considering both gravity, stress-sensitive and non-Darcy flow, the relationship between velocity and pressure can be expressed as follows (Wang and Sheng, 2017):

$$\mathbf{v}_{\alpha} = \eta_{G} \eta_{N\alpha} \mathbf{v}_{0\alpha} = \frac{\eta_{G} K_{0} k_{r\alpha}}{\mu_{\alpha}} \eta_{N} [\nabla P - \rho_{\alpha} g \nabla Z]$$
(4)

where g is the gravity, g=9.8 N/kg; Z is the depth, m; K_0 is the apparent permeability, mD; $k_{\rm r\alpha}$ is the relative permeability of phase α ; μ_{α} is the viscosity of phase α , cP; $\eta_{\rm G}$ denotes the coefficient of permeability decline due to stress sensitivity and is equal to the ratio of permeability at pressure P to K_0 ; $\eta_{\rm N}$ represents the flow rate drop coefficient caused by the non-Darcy's law. When gravity is not considered, the last term in Eq. (4) needs to be ignored. According to Gangi's law (Gangi, 1978)

$$\eta_{\rm G} = \frac{K}{K_0} = \left[1 - \left(\frac{\sigma_{\rm c} - \alpha_{\rm B} P}{\sigma_1} \right)^m \right]^3 \tag{5}$$

where α_B represents Biot's constant; σ_c stands for confining stress, Pa; σ_1 signifies the maximum effective stress leading to full fracture closure, Pa; K_0 denotes the permeability at zero confining stress, mD; m is the constant associated with fracture surface roughness. The Gangi model elucidates alterations in fracture permeability due to pressure and confining stress in fractures or fractured rock. In the model, which accounts for hydraulic fractures, natural fractures, and matrix, the decrease in formation pressure during shale oil production elevates net stress, resulting in reduced fracture aperture and an inclination towards closure. The $\eta_{N\alpha}$ in Eq. (4) can be expressed as a function of the differential pressure ∇P_{α} proposed by Wang and Sheng (2017):

$$\eta_{N\alpha} = \frac{1}{1 + a_{\alpha} e^{-b_{\alpha}|\nabla P_{\alpha}|}} \tag{6}$$

To account for the non-Darcy effect, Wang and Sheng (2017) suggested that the dimensionless coefficients a_{α} and b_{α} in the non-Darcy term of phase α can be formulated as functions connected to the apparent permeability and viscosity. This paper extends their equation to a multiphase case, for the phase α :

$$a_{\alpha} = -0.6095 \left(\frac{K_0 k_{r\alpha} \eta_G}{\mu_{\alpha}} \right)^3 + 2.5821 \left(\frac{K_0 k_{r\alpha} \eta_G}{\mu_{\alpha}} \right)^2 - 3.4594 \left(\frac{K_0 k_{r\alpha} \eta_G}{\mu_{\alpha}} \right) + 1.5836$$
 (7)

$$b_{\alpha} = 0.3603 \left(\frac{K_0 k_{r\alpha} \eta_G}{\mu_{\alpha}} \right)^2 - 0.1049 \left(\frac{K_0 k_{r\alpha} \eta_G}{\mu_{\alpha}} \right) + 1.0935$$
 (8)

Eqs. (7) and (8) reveal that the stress sensitivity and non-Darcy flow are coupled through mobility affecting parameter η_G . At constant differential pressure, a larger value of a_α represents a stronger non-Darcy effect. As the ratio of apparent permeability to viscosity increases, the non-Darcy effect in the reservoir weakens, causing the value of a_α to gradually approach 0 and η_N to approach 1. However, when the ratio of apparent permeability to viscosity exceeds 2 mD/cP, Eq. (7) indicates that the value of a_α tends to be negative, as depicted in Fig. (3).

The negative value of a_{α} may lead to a reversal of the simulated flow direction, which in turn makes the calculation not converge. Therefore, for the first time, this study employs an exponential function (Eq. (9)) to depict the relationship between a_{α} and the ratio of apparent permeability to viscosity. The exponential equation predicts a_{α} such that the model of Wang and Sheng is applicable under any mobility conditions. At higher mobility, a_{α} tends

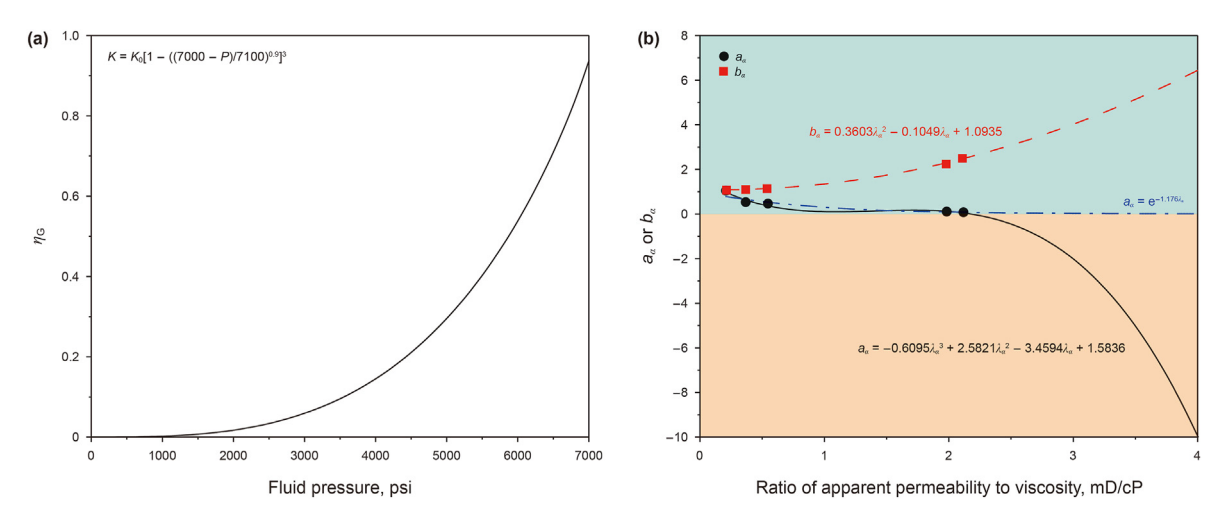


Fig. 3. Parameters of stress sensitivity and non-Darcy effect: (a) variation of stress sensitivity coefficient with fluid pressure, (b) variation of non-Darcy coefficients a_{α} and b_{α} with mobility.

towards zero, during which the flow behavior transitions from non-Darcy to Darcy flow.

$$a_{\alpha} = e^{-1.176 \left(\frac{\kappa_0 k_{r\alpha} \eta_G}{\mu_{\alpha}} \right)}$$
 (9)

To solve Eq. (1), using the backward Euler scheme for time discretization (Roe, 1986):

$$\frac{1}{\Delta t} \left\{ \left[\phi \sum_{\alpha = 0, g} \rho_{\alpha} S_{\alpha} X_{\alpha}^{i} \right]^{n+1} - \left[\phi \sum_{\alpha = 0, g} r_{\alpha} S_{\alpha} X_{\alpha}^{i} \right]^{n} \right\} + \\
\sum_{\alpha = 0, g} \nabla \cdot \left(r_{\alpha} X_{\alpha}^{i} \boldsymbol{v}_{\alpha} + J_{\alpha}^{i} \right) - \sum_{\alpha = 0, g} \nabla \cdot \left(r_{\alpha} X_{\alpha}^{i} q_{\alpha} \right) / V + q_{i}^{\text{nnc}} / V = R_{i}$$
(10)

As shown in Eq. (1) in the figure, the non-Darcy and stress sensitivity effects are related through the pressure-velocity equation, while the diffusion effect is reflected in the flux term.

The equation employs n+1 to denote the current time step, while n denotes the previous step. R_i stands for residual of component i and is assessed at the present step. This study employs the two-point flux approximation (TPFA) to discretize the temperature-pressure relationship. TPFA is a widely used numerical discretization technique for simulating fluid flow in porous media. The TPFA assumes that the flux across a grid cell interface is approximated using only the pressure values at the two adjacent cell centers. The reconstructed pressure value at the cell center is identical to the average pressure P_i within the cell. When non-Darcy flow and stress sensitivity are present, the interfacial flux v from cell i to cell k can be expressed as

$$v_{i,k} \approx \eta_G \eta_{N\alpha} T_{i,k} (P_i - P_k) \tag{11}$$

where T represents the transmissibility between cell i and cell k. The detailed derivation of this equation can be referred to in the cited literature (Aavatsmark, 2002).

3. Model development and validation

3.1. Model parameters

The numerical simulation employs parameters of the Eagle Ford

shale reservoir. The simulation integrates six pseudo-components, namely CO_2 , N_2 , C_1 , C_2 – C_5 , C_6 – C_{10} , and C_{11+} . The properties of these pseudo-components, along with their binary interaction parameters, presented in the reference (Yu et al., 2019), are used in phase behavior computations. The Peng–Robinson equation of state and flash calculation under reservoir temperature is adapted. Table 2 displays the diffusion coefficients utilized in this paper for all the pseudo-components within the liquid phase. The diffusivity values are consistent with those adopted in the study by Yu et al. (2019). The reason for not providing the gaseous diffusion coefficients is that under the pressure conditions considered in this study, there is no vapor phase present.

A 3D reservoir model including radial boreholes and hydraulic fractures is built. This paper assumes that the area after fracturing exhibiting a relatively high permeability (1 mD) (Yang S. et al., 2019). Conversely, the region beyond this zone belongs to a low-permeability shale reservoir, where the significantly low permeability enables the boundary to be regarded as a closed boundary. The vertical permeability of the matrix is set at 0.01 of the horizontal permeability. Fig. 4 shows a closed-boundary reservoir with two layers of radial boreholes, distributed along a vertical main well at the center of the reservoir. Each layer encompasses four radial boreholes positioned perpendicularly to each other.

Previous study indicates that in the presence of stress differentials, radial boreholes alter the stress distribution in the vicinity of the main well, prompting fractures to initiate along the radial boreholes. After extending for a certain distance, these fractures then gradually propagate toward the direction of the maximum principal horizontal stress (Guo et al., 2016). Therefore, this paper assumes that each radial borehole guides a single hydraulic fracture. We provide a method for approximating fracture distribution, conceptualizing fractures as a series of concatenated rectangles (Dai et al., 2023a).

The main well is cemented and does not come into direct contact with the reservoir, it is not considered within the model. Table 3 enumerates the basic reservoir properties. The fundamental reservoir parameters are consistent with those in the study by Yu et al. (2019), and references are provided for the drilling and fracturing parameters. The operational parameters of a basic case: Initially, both the upper and lower radial boreholes produce 200 d under a constant bottom-hole pressure of 2000 psi. Subsequently, the lower radial sustains production at a constant bottom-hole pressure, while the upper radial boreholes transitions into an

J.-C. Dai, T.-Y. Wang, Y. Zhang et al. Petroleum Science 22 (2025) 2950–2966

Table 2 Diffusivity of components in the liquid phase.

Diffusivity, m ² /s					
D_{CO_2}	D_{N_2}	D_{C_1}	$D_{C_2-C_5}$	$D_{C_{6}-C_{10}}$	$D_{C_{11+}}$
2.91E-10	4.13E-10	4.13E-10	1.27E-10	5.87E-11	3.60E-11

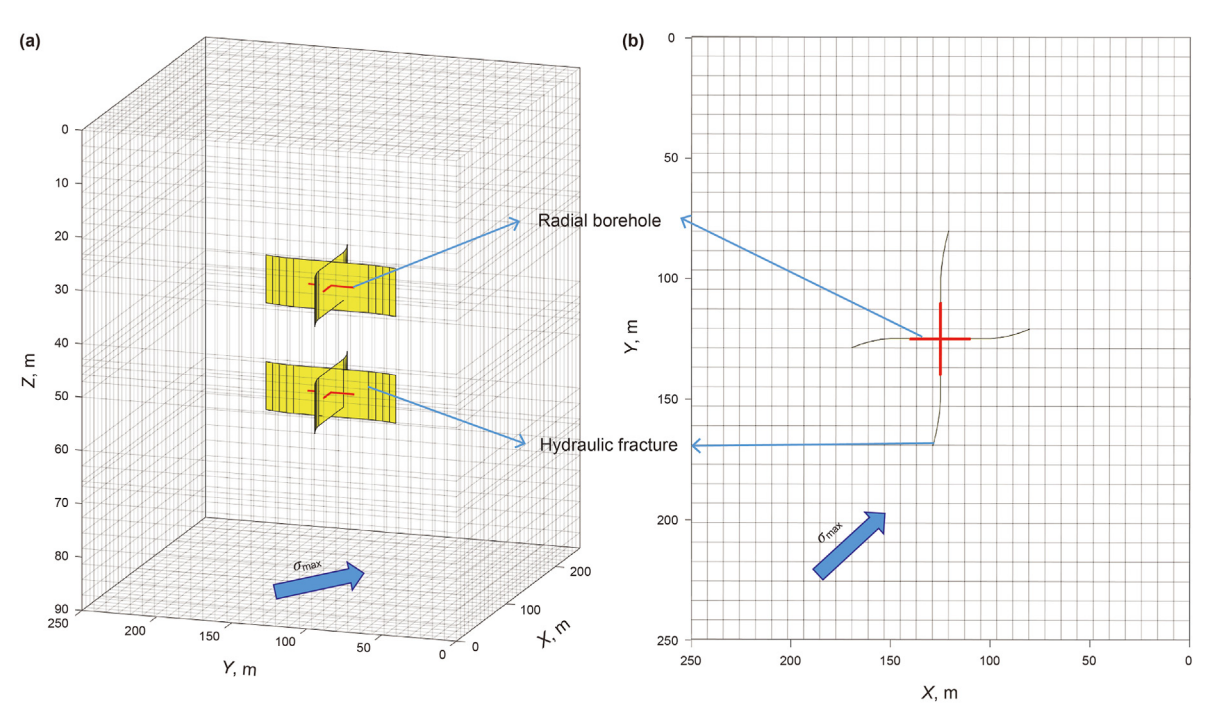


Fig. 4. Matrix, fractures, and radial borehole distribution.

Table 3 Basic reservoir properties.

Parameter	Value	Unit	Reference
Reservoir size $(X \times Y \times Z)$	250 × 250 × 90	m	
Division of gridblocks $(X \times Y \times Z)$	$41 \times 41 \times 31$	_	
Reservoir permeability (SRV)	1	mD	Yu et al. (2019)
Reservoir permeability (non-SRV)	700	mD	Yu et al. (2019)
$K_{\rm v}/K_{\rm H}$	0.01	_	Yu et al. (2019)
Porosity	10	%	Yu et al. (2019)
Tortuosity	2	_	Yu et al. (2019)
Initial reservoir pressure	7000	psi	Yu et al. (2019)
Reservoir temperature	350	°F	Yu et al. (2019)
Gangi model	$K = K_0 \left[1 - \left(\frac{7000 - P}{7100} \right)^{0.9} \right]^3$		Fitting
Initial water saturation	17	%	
Lateral length	15	m	Li et al. (2022)
Fracture half-length	100	m	Dai et al. (2023c)
Fracture height	9	m	Dai et al. (2023c)
Fracture conductivity	1400	mD·ft	Dai et al. (2023c)

injection well initiating the WAG at a constant pressure of 8000 psi. Within each 100-day WAG cycle, water is injected for the first 30 d, followed by 70 d of CO_2 injection. A water-to-gas injection time ratio is defined by the ratio of water injection duration during a cycle. The Gangi model represents the optimal fitting result obtained through validated fitting examples in Section 3.2.

3.2. Model validation

Collecting the production data from January 2010 to July 2012 during the hydraulic fracturing stages of a single well in the Eagle Ford shale condensate oil field as a benchmark, the simulation model was validated (Yang S. et al., 2019). This horizontal well was fractured into nine stages, with the production from the sixth stage

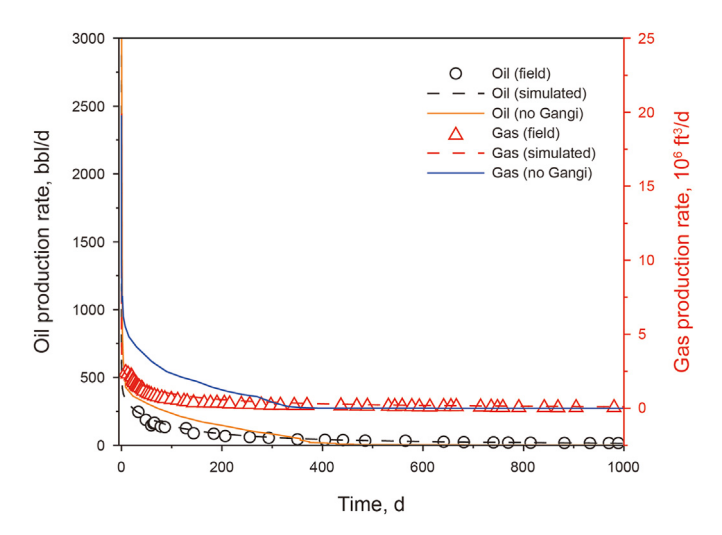


Fig. 5. Simulated data and field data of production rate over time.

used as the standard for validation. The specific parameters are as follows: dimensions of 220 ft in length, 450 ft in width, and 90 ft in height; a total of 2210 grid cells; a top layer depth of 10,000 ft; reservoir pressure of 7000 psi; matrix porosity of 0.1; matrix permeability of 0.64 mD; reservoir temperature of 347 °F; initial gas saturation of 0.65; initial water saturation of 0.35; hydraulic fracture half-length of 135 ft; hydraulic fracture height of 50 ft; initial fracture conductivity of 140 mD·ft. The bottom hole pressure, a primary constraint in the production well, was maintained at a constant 3000 psi. As shown in Fig. 5, there is a slight discrepancy between the simulated and actual oil and gas production rates, thereby demonstrating the accuracy of the numerical model in predicting oil and gas production. Ignoring stress sensitivity could lead to overestimate the production rate at initial stage.

4. Results and discussion

4.1. The effect of gravity

The gravitational segregation is crucial for WAG applied in high permeability condition. Fig. 6 illustrates the temporal variation in oil production and CO₂ production when gravity is considered. The production profile of CO₂-WAG in radial borehole fracturing

exhibits a trend of decline-increase-decline, which is similar to the pattern observed in depletion followed by water/gas injection to maintain reservoir pressure (Zhou et al., 2019; Höök et al., 2014). The entire process can be segmented into four distinct stages.

Stage I (0-200 d): Both upper and lower radial boreholes serve as production wells. The pressure depletion results in a rapid decline in oil production to 0.437% of the initial value after 200 d

Stage II (200–600 d): One layer of radial boreholes turns to WAG mode. The reduced number of production boreholes results in a sudden decline in the oil production rate at the beginning of Stage II. As the reservoir pressure gradually recovers, the oil production rate increases. The $\rm CO_2$ produced is naturally present in the reservoir in Stages I and II.

Stage III (600—1200 d): The injected CO₂ flows through the oil reservoir between the radial boreholes and begins to be produced from the production boreholes (Khan and Mandal, 2020). However, it constitutes a relatively small proportion of the produced substances. The oil production rate continues to increase, reaching its peak at 287.4 bbl/d on the 1200th day.

Stage IV (1200–6000 d): As the ratio of CO₂ in the produced substances increases over time and the rate of CO₂ production climbed, the oil production rate declined. The amount of CO₂ production in Stages III and IV represents the degree of gas channeling.

Due to the vertical alignment of radial boreholes, fluid movement is largely governed by vertical pressure gradients, with fluid flow primarily occurring in the vertical direction, same as gravity direction. Therefore, no significant separation occurs. Consequently, the influence of gravity on the segregation of oil and $\rm CO_2$ production is comparatively minor, as shown in Fig. 6. Furthermore, gravitational segregation exerts a limited influence on the production of both oil and $\rm CO_2$. This effect typically becomes significant only when the permeability exceeds 10 mD (Khan and Mandal, 2020; Faisal et al., 2009).

Injecting water and CO_2 from the top layer can be more advantageous for their downward migration. Consequently, on the 6000th day, the cumulative oil production and CO_2 production from upper injection case are respectively 1.85% and 5.85% higher than that of lower injection case. When gravity is not considered, CO_2 and water are less prone to migration after injection, leading to a decline in injectivity and resulting in a lower oil and CO_2

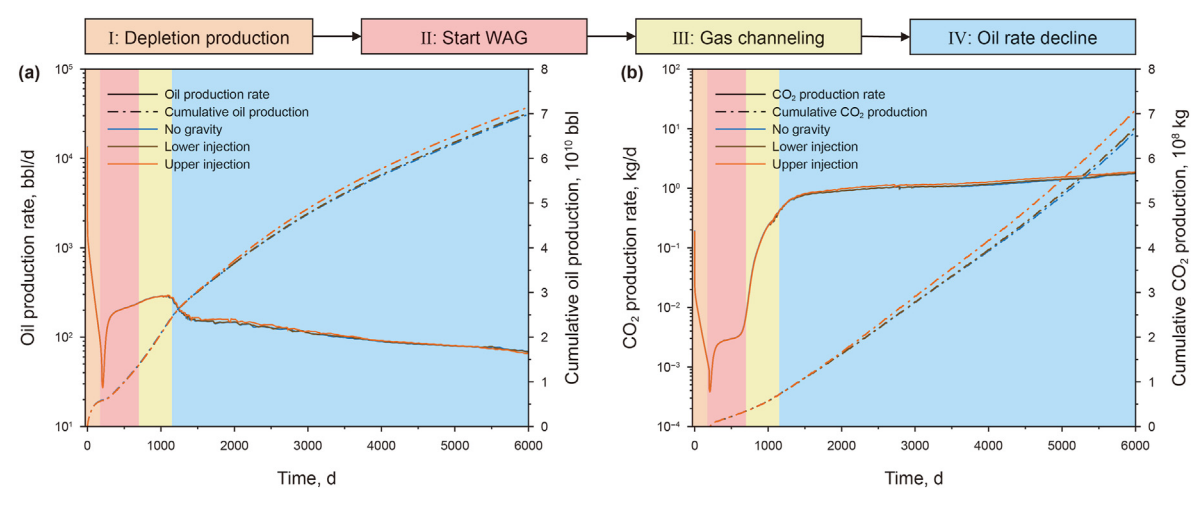


Fig. 6. Effect of CO₂ injection directions on WAG performance over time: (a) oil production, (b) CO₂ production.

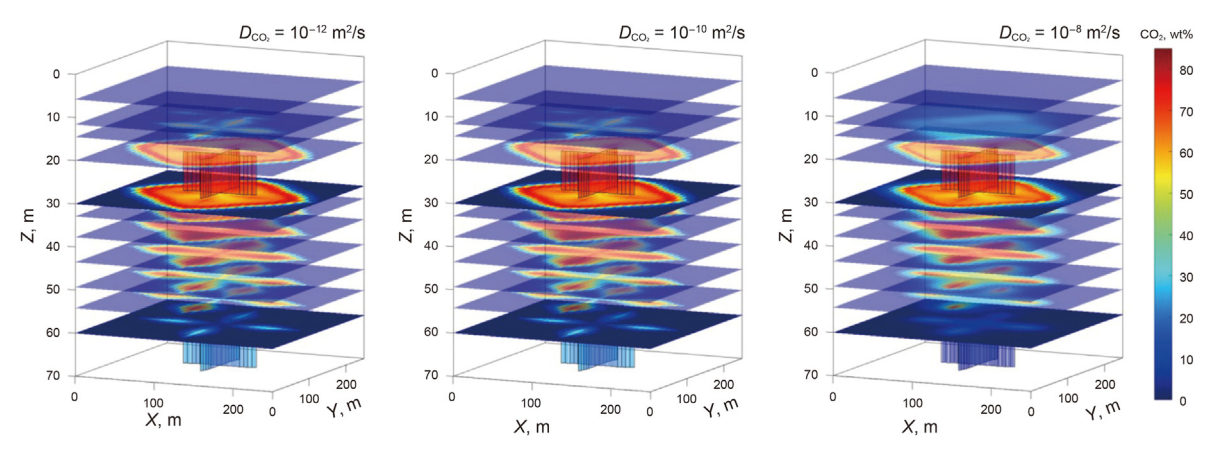


Fig. 7. CO₂ distribution in the reservoir under different diffusion coefficients on the 1000th day.

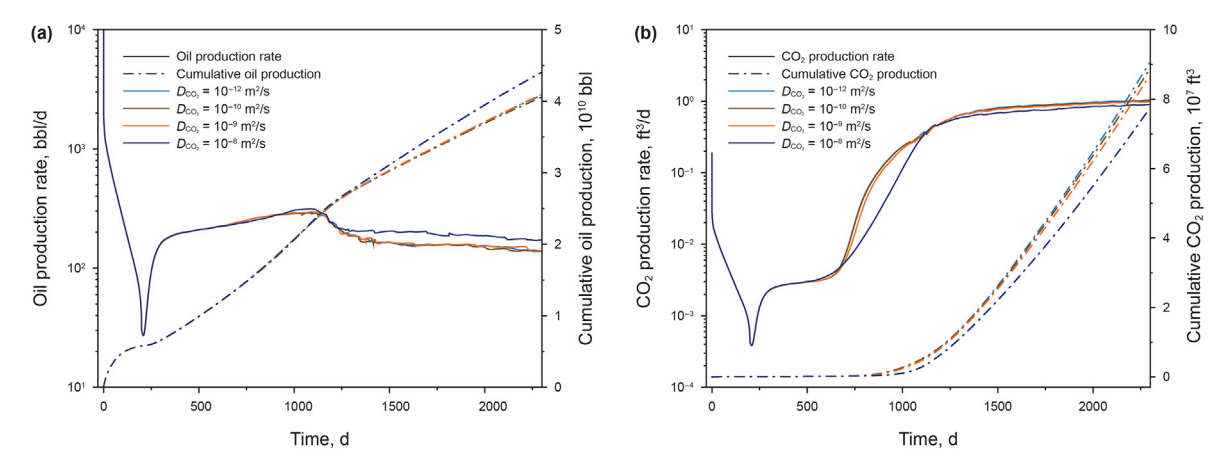


Fig. 8. Effects of CO₂ diffusion coefficient on WAG performance over time: (a) oil production, (b) CO₂ production.

production when gravity is considered. All subsequent discussion in this paper takes into account gravity, with CO₂ being injected from the upper radial borehole.

4.2. The effect of diffusion

The intensity of the diffusion effect of CO_2 is directly proportional to the gradient of CO_2 concentration. Although its intensity is relatively smaller compared to the pressure gradient, it plays a dominant role in areas where the pressure gradient is small and the CO_2 concentration gradient is large.

As shown in Fig. 7, in addition to the flow driven by pressure gradients, a higher diffusion coefficient indicates a stronger ability of CO_2 to migrate under concentration difference. Consequently, some of the injected CO_2 migrates towards the top and outward to the boundary region of the reservoir, leading to a decrease in the amount of CO_2 moving downwards driven by the pressure gradient, thus resulting in a reduction of CO_2 production and a more extensive distribution of CO_2 . Previous study of CO_2 huff-and-puff simulation shows that a higher CO_2 diffusion coefficient $(10^{-8}-10^{-6} \text{ m}^2/\text{s})$ leads to a more extensive distribution of CO_2 (Yu et al., 2019), which is consistent with the findings of this study.

Owing to the increased migration of CO₂ towards the periphery of the reservoir, the amount of CO₂ reaching the production layer is reduced. Therefore, as depicted in Fig. 8(b), the cumulative CO₂ production with a $D_{\rm CO_2}$ of 10^{-8} m²/s amounts to 85.47% of that achieved with a $D_{\rm CO_2}$ of 10^{-12} m²/s. In addition, the CO₂ migrating

due to diffusion causes an increase in pressure in the upper and surrounding area of the central axis, enhancing the tendency of fluid flow downwards and towards the vertical well, thus increasing oil production. As shown in Fig. 8(a), the cumulative oil production at a $D_{\rm CO_2}$ of 10^{-8} m²/s is 1.07 times that when the $D_{\rm CO_2}$ is 10^{-12} m²/s. A diffusion coefficient of 10^{-10} m²/s for CO₂ is applied in the subsequent analyses of this study. The phenomenon of a limited effect on decreasing CO₂ production and increasing oil production under high permeability conditions is consistent with the results in previous studies of CO₂ huff-and-puff and displacement (Jia et al., 2019b). Moreover, the influence of CO₂ diffusion becomes significant only when the permeability is relatively low (Jia et al., 2019a).

4.3. The effect of stress sensitivity and non-Darcy effect

The permeability reduction caused by stress sensitivity is a function of reservoir pressure. Fig. 9 shows the distribution of $\eta_{\rm G}$ over time. At the end of depletion production, due to the decrease in reservoir pressure, $\eta_{\rm G}$ is less than 27.3% throughout the entire oil reservoir. Upon initiation of WAG, the pressure near the injection well rises to the injection pressure, forming a gradually decreasing pressure gradient from the injection layer to the production layer vertically.

The increase in pressure causes η_G to rise, indicating an increase in the permeability. For example, on the 6000th day, η_G is 95.1% around the injection radial borehole, while it remains at 34.5% around the production boreholes. Therefore, as shown in Fig. 10(b),

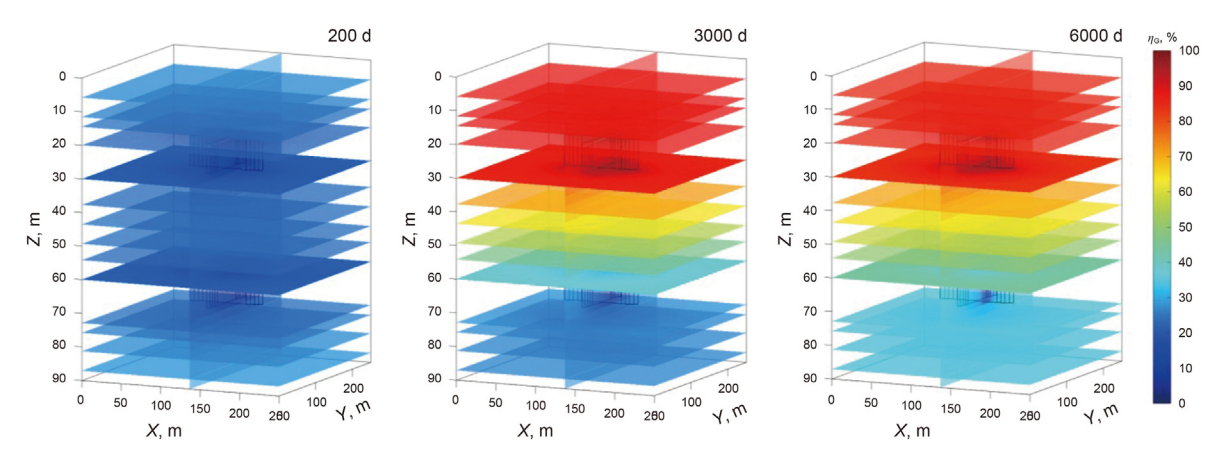
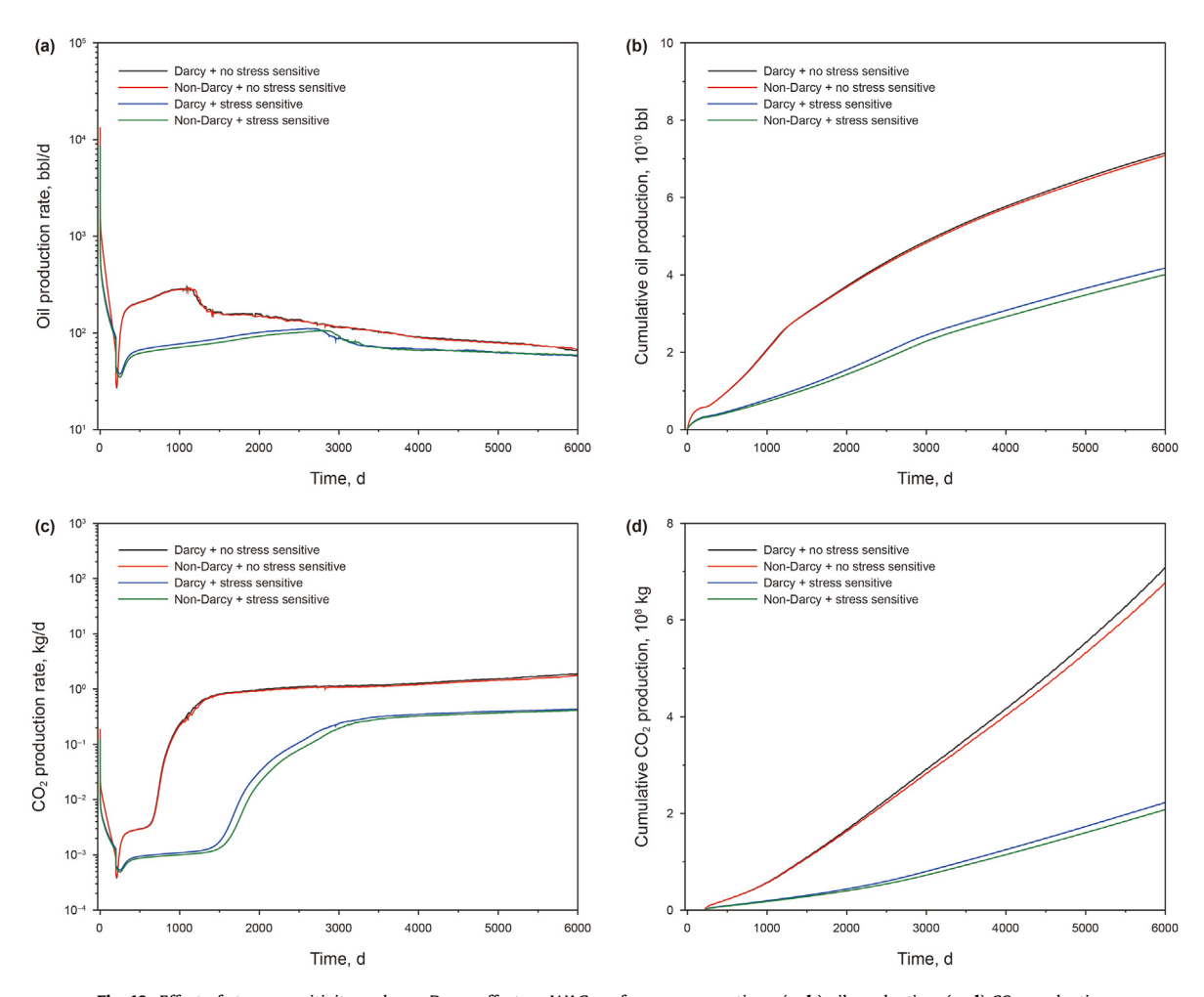


Fig. 9. The spatial distribution of η_G over time under stress sensitivity effect.



 $\textbf{Fig. 10.} \ \ \textbf{Effect of stress sensitivity and non-Darcy effect on WAG performance over time:} \ \textbf{(a, b)} \ oil \ production, \ \textbf{(c, d)} \ CO_2 \ production.$

when the stress sensitivity is present, the cumulative oil production is 58.4% of that when the stress sensitivity is not considered. Previous study shows that the production under stress-sensitive conditions typically decreases by approximately 50% (Cui et al., 2021; Jiang and Yang, 2018). However, the stress sensitivity extends the time from the start of WAG to gas breakthrough.

The flow velocity decay coefficient η_N , resulting from non-Darcy's law, is a function of pressure difference and saturation. Using

the water phase as an example, at the end of the depletion stage, the pressure differences are small except around the production layer, where $\eta_{\rm Nw}$ is about 50%, as shown in Fig. 11. When WAG starts and vertical pressure gradient is established, the vertical $\eta_{\rm Nw}$ between the injection and production layers recovers to 60%–99%, while the $\eta_{\rm Nw}$ in areas outside the injection and production layers remains around 50%.

Different $\eta_{\rm Nw}$ value is also affected by water saturations. A lower

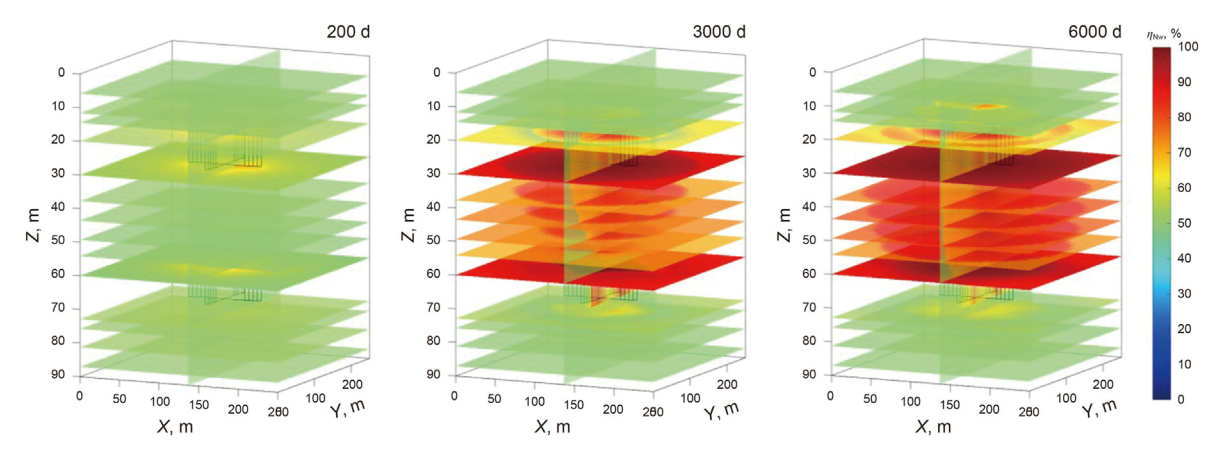


Fig. 11. The distribution of η_{Nw} over time under non-Darcy effect.

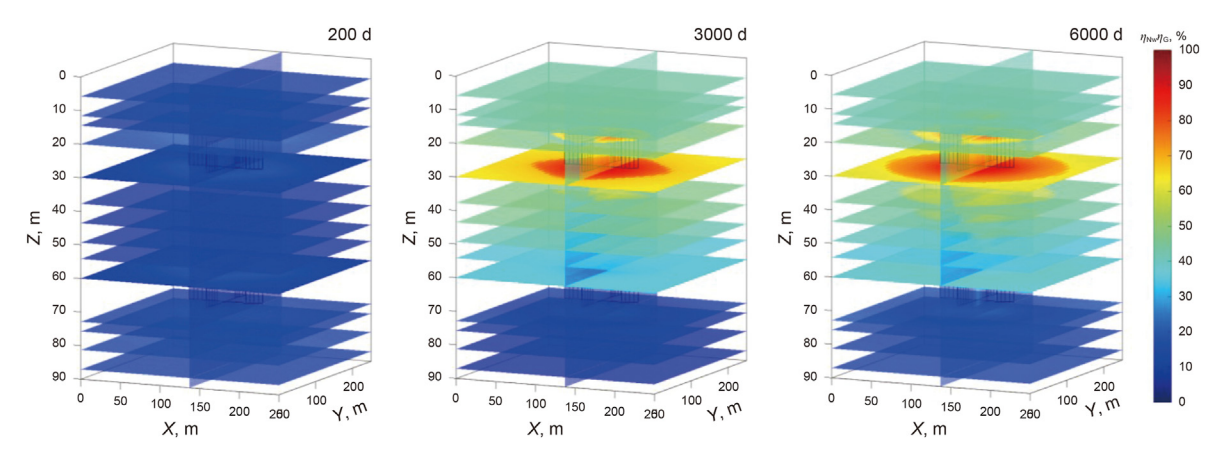


Fig. 12. The distribution of $\eta_G\eta_{Nw}$ on 200th, 3000th, and 6000th day.

water saturation leads to a reduction in the relative permeability of the water phase. The water saturation is less at locations far from the main well and the injection layer, so the area with larger $\eta_{\rm Nw}$ values show an inverted cone-shaped distribution. As shown in Fig. 12, when considering non-Darcy's law, oil production and CO₂ production are 96% and 99%, respectively, of the values when considering Darcy's law. The relatively minor impact of non-Darcy flow on production can be attributed to the overall high permeability of the reservoir.

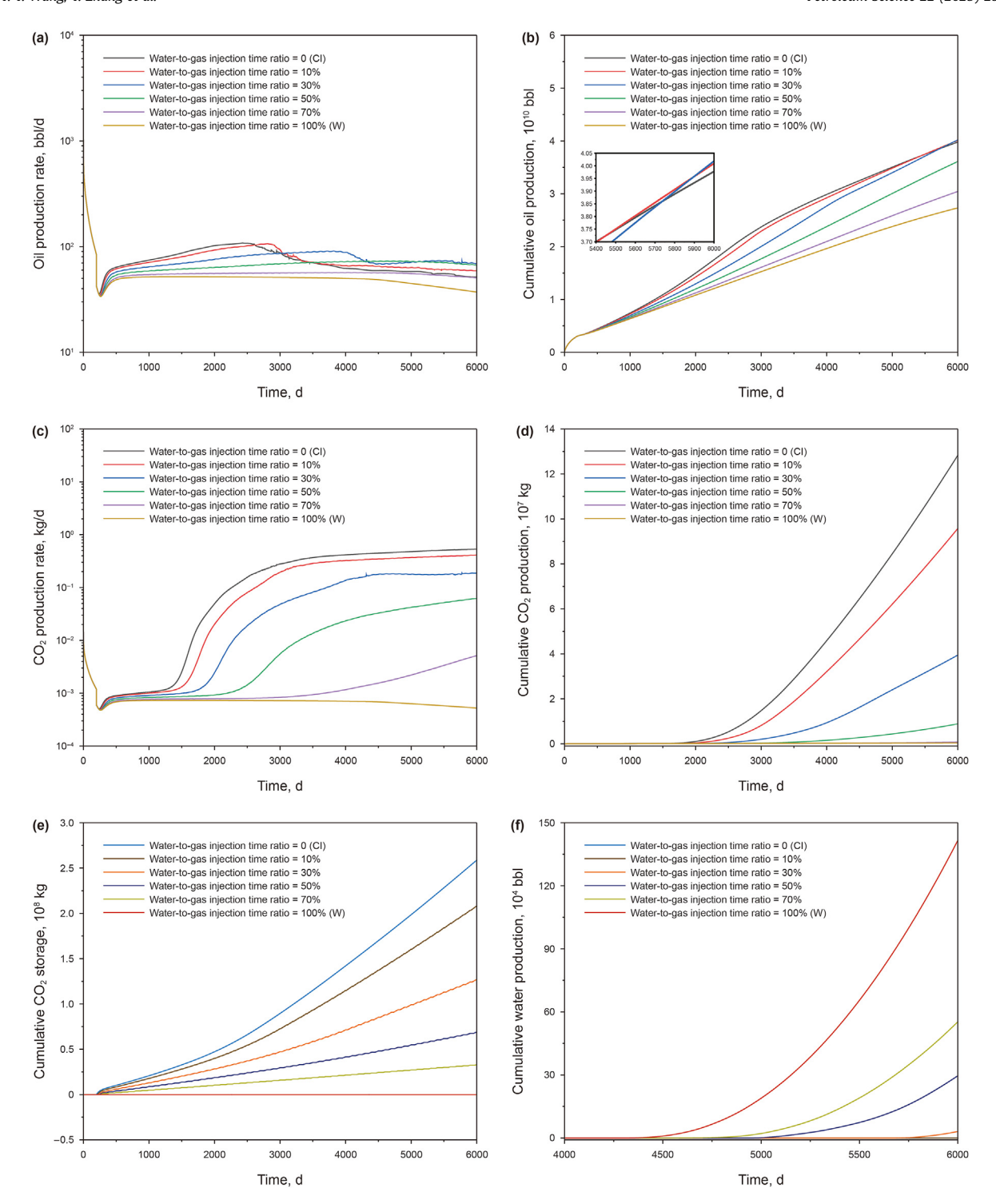
When both stress sensitivity and the non-Darcy effect are considered, a distribution of flow velocity decay coefficient $\eta_N \eta_G$ is shown in Fig. 12. At the end of the depletion stage, the range of $\eta_{Nw}\eta_{G}$ is between 0 and 21.2%. After WAG starts, $\eta_{Nw}\eta_{G}$ increases with the growth of pressure and pressure difference. In this case, the distribution of the $\eta_{\rm Nw}\eta_{\rm G}$ value combines the characteristics of stress-sensitive and non-Darcy flow, showing a higher value area (not strongly affected by stress sensitivity and the non-Darcy effect) around the injection layer and a gradual shrink towards the production layer. On the 6000th day, the range of $\eta_{Nw}\eta_{G}$ rises to between 0 and 92.1%. This shows that when stress sensitivity and non-Darcy's law coexist, the $\eta_{Nw}\eta_G$ is not simply the product of η_{Nw} and η_G when they are considered separately. When stress sensitivity and non-Darcy's law are coupled, the cumulative oil production is 55.9% of the cases where neither is considered, and the time duration from WAG beginning to gas breakthrough is three times longer. The result demonstrates that the non-Darcy effect is more pronounced in the presence of stress sensitivity, resulting in lower production rate when both effects coexist. This finding is

consistent with the results reported by Dong et al. (2019). Stress sensitivity and non-Darcy flow are taken into account in the following analysis.

4.4. The effect of water-to-gas injection time ratio

Fig. 13 shows the variation in production rate over time for water-to-gas injection time ratio ranging from 0 (CI) to 100% (continuous water injection). Because $K_{\rm r}$ of water and ${\rm CO_2}$ are different, at the same injection pressure, the rate of gas injection is slightly higher than the water injection rate, resulting in a fluctuating rate over time. Meanwhile, due to the low viscosity of sc-CO₂, ${\rm CO_2}$ flows more easily than water. Therefore, the larger the proportion of ${\rm CO_2}$ injection time, the lower the mobility ratio is, more likely that gas breakthrough occurs. As shown in Fig. 14, the mass fraction of ${\rm CO_2}$ is about 50% for WAG with 30% water-to-gas injection time ratio, while it is over 80% for CI. However, the distribution of ${\rm CO_2}$ in WAG is more uniform, which can effectively slow down the gas breakthrough. The time before gas breakthrough in CI case is 500 d less than that of WAG with 30% water-to-gas injection time ratio.

In the case with a 30% water-to-gas injection time ratio, the amount of gas breakthrough decreases, subsequently causing a slight increase in oil production. However, after 5660 d, water breakthrough occurred, leading to a decline in the rate of oil production. On the 6000th day, the oil production rate during CI is 87.2% of that observed in WAG with a 30% water-to-gas injection time ratio, resulting in a cumulative oil production reduction of



 $\textbf{Fig. 13.} \ \ \textbf{Effect of water-to-gas injection time ratio on WAG performance over time: (a, b) oil production, (c, d, e) CO_2 production and storage, (f) water production. \\$

 3.5×10^8 bbl. However, because the amount of CO_2 injected during CI is the largest, its CO_2 storage volume on the 6000th day is the greatest, being 2.04 times that of WAG with a 30% water-to-gas injection time ratio. During continuous water injection, a water breakthrough also occurs on the 4250th day, and the oil displacement performance of water is worse than CO_2 . Therefore, on the 6000th day, the oil production volume of continuous water injection case is only 53.7% of that for WAG with 30% water-to-gas injection time ratio.

In the optimization of WAG parameters for the Pubei Oilfield reservoir by Chen et al. (2010), various injection modes are compared, including continuous gas injection, continuous water injection (which yielded the lowest recovery), water injection followed by gas injection, and gas injection followed by water injection. They concluded that the optimal recovery was achieved with a WAG ratio of 1:2, which is similar to the findings of this study. Depending on the reservoir type and permeability, the WAG ratio may vary from higher than 4:1 to 1:1 (Afzali et al., 2018; Ghaderi

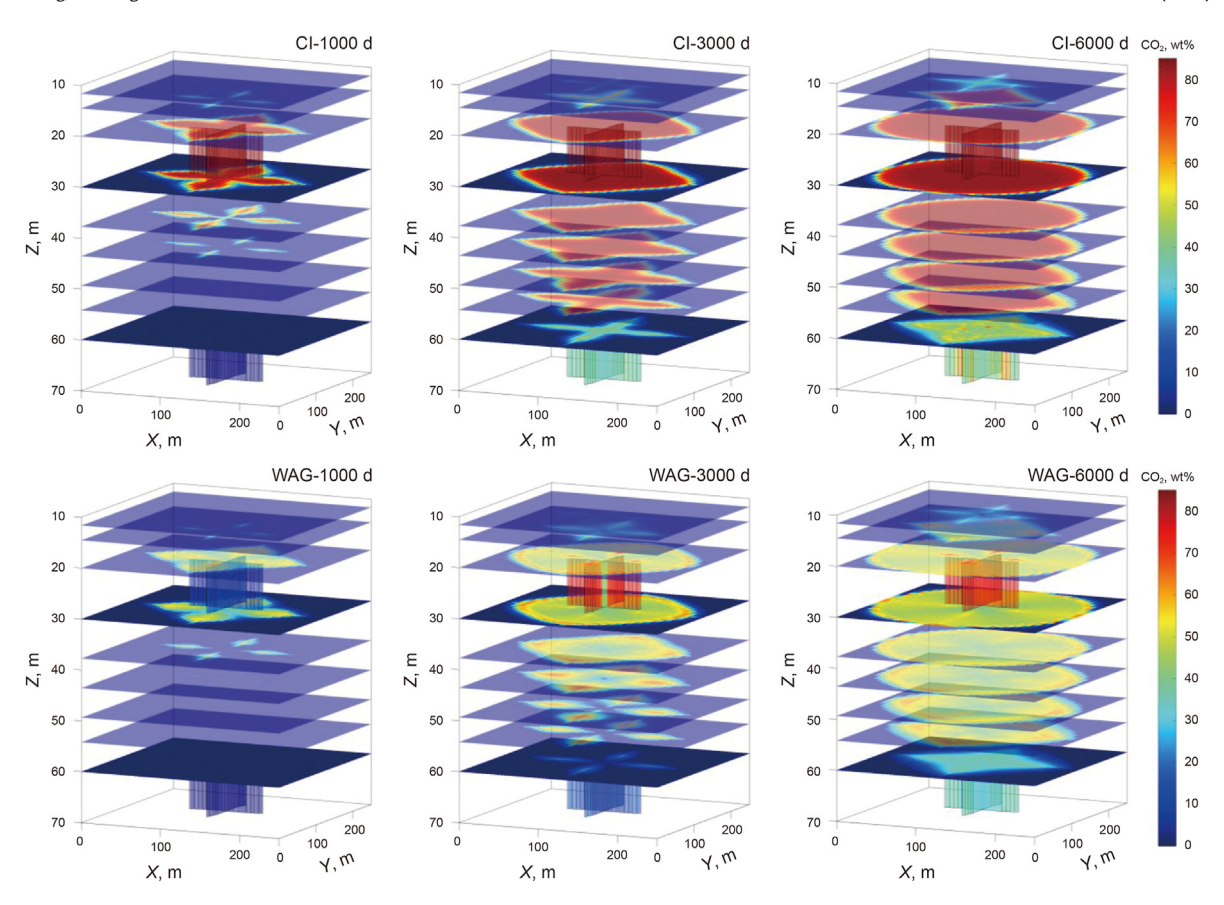


Fig. 14. CO₂ distribution in the reservoir over time under continuous CO₂ injection and WAG with a 30% water-to-gas injection time ratio.

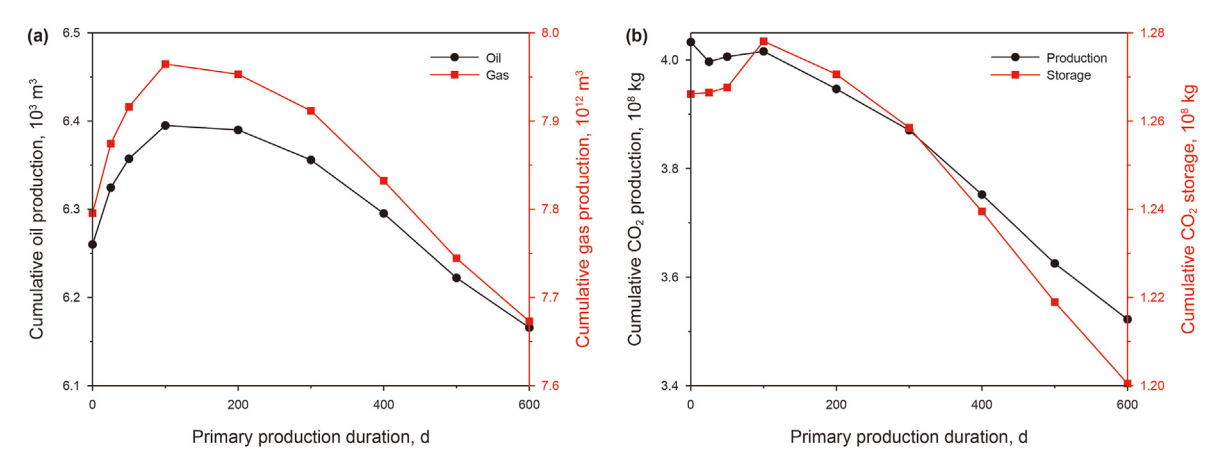


Fig. 15. Effect of primary production duration on WAG performance: (a) oil and gas production, (b) CO_2 production and storage.

et al., 2012b), but its production rate is always greater than that of CI. Therefore, for subsequent discussion, WAG with a 30% water-togas injection time ratio is chosen for the following discussion.

4.5. The effect of primary production duration

The primary production duration, or the period before the start of WAG injection, is a critical operational factor affecting the reservoir pressure. The longer the primary production duration, the greater the extent of reservoir pressure depletion, and the more pronounced the effects of stress sensitivity and non-Darcy effect. When the total time duration is fixed, a reduced WAG time duration

leads to a decrease in the volume of injected CO₂, thereby causing insufficient recovery of reservoir pressure. As shown in Fig. 15, when the initial primary production duration exceeds 100 d, oil production, CO₂ production, and CO₂ storage amount all decrease with the increase in initial production time. However, if the primary production duration is too short, the high oil production rate at the beginning of depletion production cannot be fully utilized. Therefore, as shown in Fig. 15(a), the maximum oil and gas production is achieved at 100 d. In conclusion, the subsequent discussion is based on an initial production time of 100 d. The concave-upward curve of oil and gas production rates varying with depletion time is consistent with previous studies, with the optimal value depending

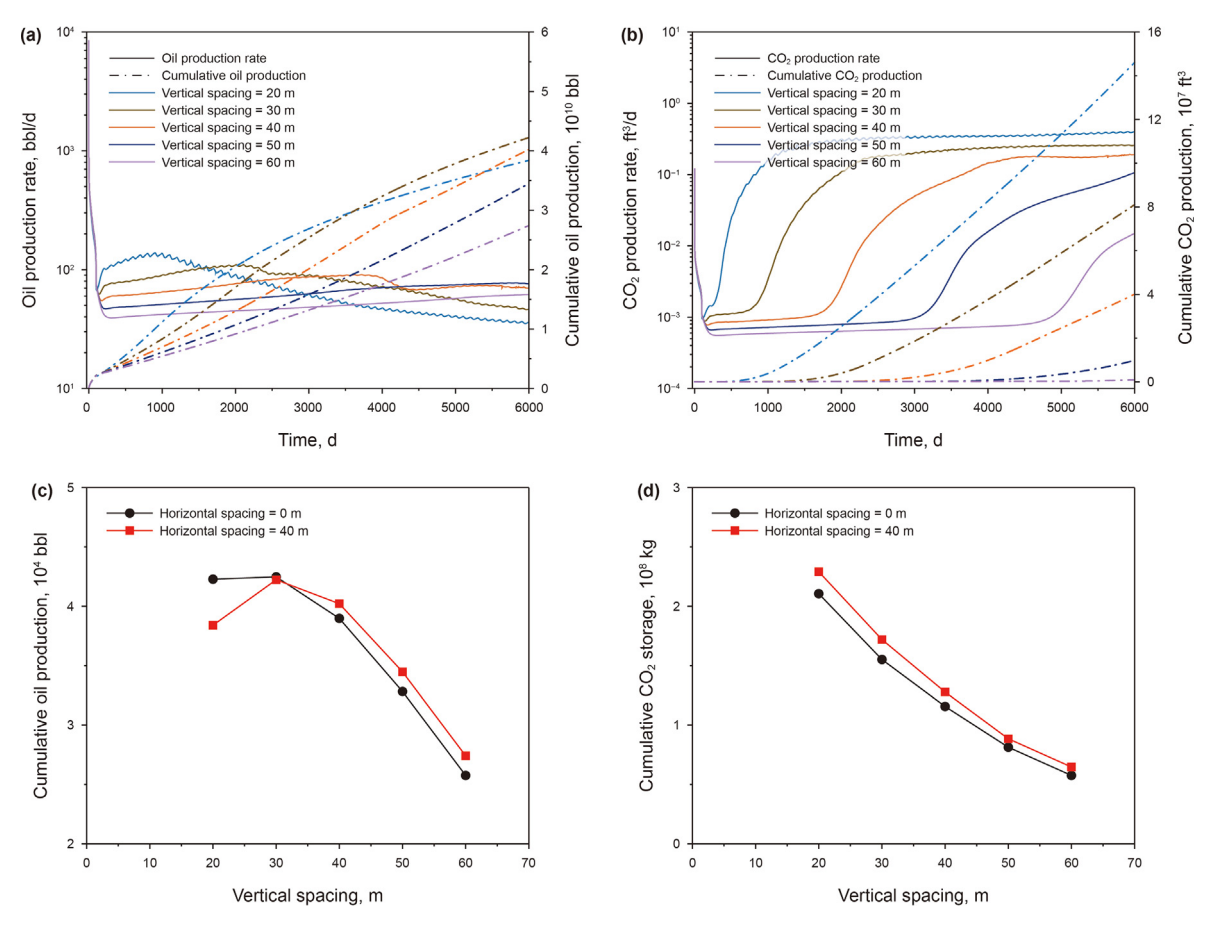


Fig. 16. Impact of well spacing on WAG performance: variations of oil (a) and CO₂ (b) production over time, and variations of cumulative oil production (c) and CO₂ storage (d) with well spacing.

on the size of the reservoir and the type of reservoir boundaries (Chen and Gu, 2017; Sheng, 2017).

4.6. The effect of spacing between radial borehole layers

The relative position between the two layers is an essential parameter in the design of radial borehole fracturing. The definition of vertical spacing is the distance between the upper and lower radial boreholes projected onto the vertical plane, while horizontal spacing is the distance projected onto the horizontal plane. When the pressures of the injection and production layers are kept constant, increasing the spacing between layers reduces the pressure gradient while also enhancing the non-Darcy effect, resulting in decreased CO₂ injection and oil production rates. However, enlarging the layer spacing increases the flow distance for CO₂, leading to an increased duration before gas breakthrough.

When the vertical spacing between wells is less than 20 m, the early gas breakthrough causes a decrease in the oil production rate, as shown in Fig. 16(a). The cumulative oil production of the case with a vertical spacing of 20 m is 91% of that at a vertical spacing of 30 m on the 6000th day. The latter mitigates the CO_2 breakthrough time by 500 d compared to the former. Previous research identifies that excessively close well spacing can lead to early water breakthrough (Zhang et al., 2017), while overly wide well spacing results in an insufficient pressure gradient (Nwachukwu et al., 2018). These findings validate the rationality of the layer spacing results presented in this study.

The effect of reducing the vertical spacing on the CO₂ injection rate is greater than its effect on the CO₂ production rate, reducing

the vertical spacing is more beneficial for CO_2 storage. As shown in Fig. 16(b), the cumulative CO_2 production on the 6000th day of the case with 20 m vertical spacing is 1.33 times that at a vertical spacing of 30 m. The effect of horizontal spacing is generally consistent with the effect of vertical spacing. However, because the horizontal permeability of the reservoir is higher than the vertical permeability, increasing the horizontal layer spacing has a small impact on oil production and CO_2 storage (Fig. 16(c) and (d)).

4.7. Comparison of radial borehole fracturing and horizontal well fracturing

Radial borehole fracturing is based on vertical wells and has a lower implementation cost compared to horizontal well drilling and fracturing. In previous studies, we compared the applicability of radial borehole fracturing and horizontal well fracturing in a depletion case (Dai et al., 2023a) and a CO₂ huff-and-puff case (Dai et al., 2023c). The findings indicated that, radial borehole fracturing changes the flow direction, making it more suitable under conditions of low vertical permeability and limited hydraulic fracture height. In this study, a simplified horizontal well fracturing case was established. The horizontal wells have length of 200 m, a diameter of 300 mm, and a well spacing of 200 m. The relative position on the Z axis was 45 m. The fractures are evenly distributed along the horizontal well with a fracture length of 20 m and a fracture height of 9 m. Other parameters are consistent with those of radial borehole fracturing. The parameters for radial borehole fracturing are same as those described earlier, with the two wells positioned as shown in Fig. 17. The production parameters for both

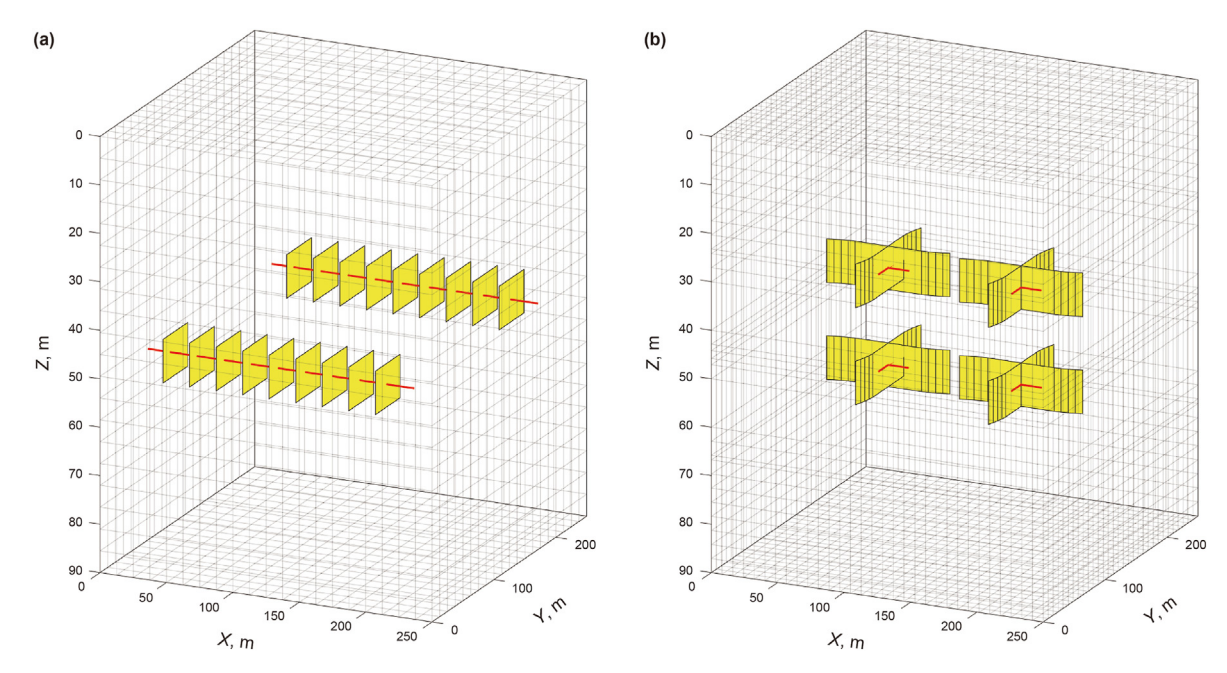


Fig. 17. (a) Two fractured horizontal wells with nine fracture stages each and (b) two vertical wells with radial fracturing.

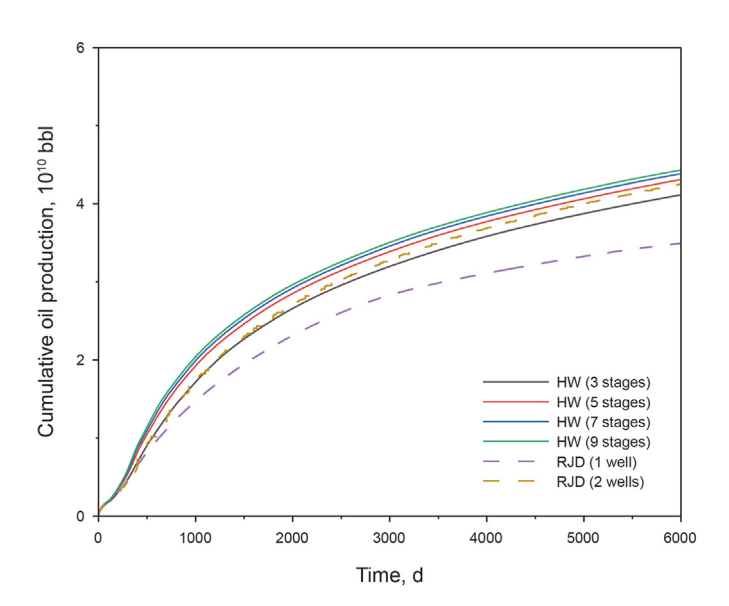


Fig. 18. Comparison of cumulative oil production between radial borehole fracturing and horizontal well fracturing in WAG operations. HW represents horizontal well hydraulic fracturing. RJD represents radial borehole fracturing.

cases are consistent with those described previously.

As shown in Fig. 18, when the number of main wells for radial borehole fracturing is one, the production is only 84.87% of that of three-stage fractured horizontal well. When the number of main wells for radial borehole fracturing is two, its oil production is comparable to that of five-stage fractured horizontal wells. When the length of horizontal wells is kept constant and the number of stages increases, the increase in oil production diminishes. In contrast, the deployment of vertical wells with radial fracturing is more flexible. Therefore, when the horizontal well fracturing is not economically viable in reservoirs with dispersed dessert, that is, when the well length is limited, radial borehole fracturing can be considered as a supplementary or alternative option.

5. Conclusions

To reduce the degree of water—gas separation during the WAG process and lower costs, this study first introduces a novel approach to apply WAG in a vertical well with radial borehole fractures. A compositional model is built to analyze the influences of gravity, diffusion, stress sensitivity, and non-Darcy effect on fluid flow. This study highlights the issue of negative values in the exponential non-Darcy law at high mobility. Furthermore, the effects of the water-to-gas injection time ratio, primary production duration, and layer spacing on oil production, gas breakthrough, and CO₂ storage volumes are investigated. Main findings are as follows.

- (1) The radial borehole fracturing-WAG operation can be divided into four distinctive stages, each marked by specific oil and CO₂ production trends. Unlike traditional WAG schemes, the radial borehole fracturing-WAG approach aligns the direction of pressure gradients vertically, thereby substantially reducing the influence of gravity on production capacity. Moreover, under conditions of high permeability, the impact of CO₂ diffusion is also insignificant.
- (2) This study reveals the distribution of pesudo permeability when the exponential non-Darcy law and stress sensitivity coexist. The reduction in apparent permeability reaches to 22% during the depletion production stage. After the initiation of WAG, the unaffected regions are located around the injection layer, with a gradual shrinkage towards the production well. The presence of stress sensitivity enhances the influence of the non-Darcy effect.
- (3) WAG with a 30% water-to-gas injection time ratio can provide the highest cumulative oil production, delay gas breakthrough, and achieve more evenly distributed CO₂ within the reservoir. While continuous CO₂ injection initially yields high oil production but experiences a rapid decline after gas breakthroughs, resulting in lower cumulative oil production over time.
- (4) The initial production period before WAG injection determines the magnitude of the average reservoir pressure,

J.-C. Dai, T.-Y. Wang, Y. Zhang et al. Petroleum Science 22 (2025) 2950–2966

while the vertical distance between wells determines the magnitude of the pressure gradient. These two factors are respectively associated with stress sensitivity and non-Darcy effects. The initial production period, well spacing, and oil production exist optimal values.

- (5) This study compares radial borehole fracturing and horizontal well fracturing in WAG operations, finding that radial borehole fracturing yields slightly lower production than five-stage fractured horizontal well fracturing when the number of main wells is two, indicating that radial borehole fracturing can serve as an alternative or supplement to horizontal well fracturing when the dessert volume is limited.
- (6) Limitations: The numerical model utilized in this study still has shortcomings in simulating the WAG process, such as overlooking capillary forces, the dissolution of CO₂ in water, and the mechanism of wettability hysteresis. For instance, when CO₂ dissolves in water, it alters the water density, viscosity, and oil—water relative permeability, thereby affecting the fluid flow processes. In the future, we will further analyze the impact of the above factors on the WAG.

CRediT authorship contribution statement

Jia-Cheng Dai: Writing — original draft, Validation, Methodology. **Tian-Yu Wang:** Project administration, Funding acquisition. **Ye Zhang:** Validation, Software, Funding acquisition. **Zhi-Ping Zhang:** Supervision, Project administration, Data curation. **Chun-Lin Zeng:** Validation, Software, Conceptualization. **Kang-Jian Tian:** Writing — review & editing, Visualization, Formal analysis. **Jing-Bin Li:** Methodology, Investigation, Conceptualization. **Shou-Ceng Tian:** Supervision, Resources, Funding acquisition. **Gen-Sheng Li:** Supervision, Resources, Methodology.

Declaration of interests

The authors declare that they have no known competing financial interests or personal relationships that could have appeared to influence the work reported in this paper.

Acknowledgements

This study has been funded by the Young Scientists Fund of the National Natural Science Foundation of China (52204063), and the Key Laboratory of Shale Gas Exploration, Ministry of Natural Resources (Chongqing Institute of Geology and Mineral Resources), Chongqing, China (KLSGE-202202). Moreover, we would like to express our heartfelt appreciation to the Computational Geosciences Group in the Department of Mathematics and Cybernetics at SINTEF Digital for developing and providing the free open-source MATLAB Reservoir Simulation Toolbox (MRST) used in this research.

References

- Aavatsmark, I., 2002. An introduction to multipoint flux approximations for quadrilateral grids. Comput. Geosci. 6, 405–432. https://doi.org/10.1023/A: 1021291114475
- Afzali, S., Rezaei, N., Zendehboudi, S., 2018. A comprehensive review on enhanced oil recovery by water alternating gas (WAG) injection. Fuel 227, 218–246. https://doi.org/10.1016/j.fuel.2018.04.015.
- Afzali, S., Ghamartale, A., Rezaei, N., et al., 2020. Mathematical modeling and simulation of water-alternating-gas (WAG) process by incorporating capillary pressure and hysteresis effects. Fuel 263, 116362. https://doi.org/10.1016/ i.fuel.2019.116362.
- Afari, S., Ling, K., Sennaoui, B., et al., 2022. Optimization of CO₂ huff-n-puff EOR in the Bakken Formation using numerical simulation and response surface methodology. J. Petrol. Sci. Eng. 215, 110552. https://doi.org/10.1016/

j.petrol.2022.110552.

- Altawati, F., Emadi, H., Pathak, S., 2021. Improving oil recovery of Eagle Ford shale samples using cryogenic and cyclic gas injection methods-An experimental study. Fuel 302, 121170. https://doi.org/10.1016/j.fuel.2021.121170.
- Asante, J., Ampomah, W., Tu, J., et al., 2024. Data-driven modeling for forecasting oil recovery: a timeseries neural network approach for tertiary CO₂ WAG EOR. Geoenergy Sci. Eng. 233, 212555. https://doi.org/10.1016/j.geoen.2023.212555.
- Awolayo, A.N., Norton, H., de Obeso, J.C., et al., 2025. Water-Alternating-Gas (WAG) injection scheme for enhancement of carbon dioxide mineralization in basaltic aquifers. Fuel 385, 134127. https://doi.org/10.1016/j.fuel.2024.134127.
- Bruni, M.A., Biasotti, J.H., Salomone, G.D., 2007. Radial drilling in Argentina. In: Latin American & Caribbean Petroleum Engineering Conference. https://doi.org/10.2118/107382-MS.
- Caineng, Z., Yang, Z., Cui, J., et al., 2013. Formation mechanism, geological characteristics and development strategy of nonmarine shale oil in China. Petrol. Explor. Dev. 40 (1), 15–27. https://doi.org/10.1016/S1876-3804(13)60002-6.
- Callahan, K., Goudarzi, L., Wallace, M., et al., 2014. A review of the CO₂ pipeline infrastructure in the US. https://doi.org/10.2172/1487233.
- Chen, C., Gu, M., 2017. Investigation of cyclic CO₂ huff-and-puff recovery in shale oil reservoirs using reservoir simulation and sensitivity analysis. Fuel 188, 102–111. https://doi.org/10.1016/i.fuel.2016.10.006.
- https://doi.org/10.1016/j.fuel.2016.10.006.

 Chen, S., Li, H., Yang, D., et al., 2010. Optimal parametric design for wateralternating-gas (WAG) process in a CO₂-miscible flooding reservoir. J. Can. Petrol. Technol. 49 (10), 75–82. https://doi.org/10.2118/141650-PA.
- Cheng, H., Wang, F., Guan, X., et al., 2023. A mathematical model for pre-Darcy flow in low permeability porous media with stress sensitivity and the boundary-layer effect. Eng. Geol. 324, 107257. https://doi.org/10.1016/j.enggeo.2023.107257.
- Claridge, E.L., 1982. CO₂ flooding strategy in a communicating layered reservoir. J. Petrol. Technol. 34 (12), 2746–2756. https://doi.org/10.2118/10289-PA.
- Cui, Y., Jiang, R., Wang, Q., et al., 2021. Production performance analysis of multi-fractured horizontal well in shale gas reservoir considering space variable and stress-sensitive fractures. J. Petrol. Sci. Eng. 207, 109171. https://doi.org/10.1016/j.petrol.2021.109171.
- Dai, J., Wang, T., Tian, K., et al., 2023a. CO₂ flooding in shale oil reservoir with radial borehole fracturing for CO₂ storage and enhanced oil recovery. Pet. Sci. 21 (1), 519–534. https://doi.org/10.1016/j.petsci.2023.08.033.
- Dai, J., Zheng, Z., Wang, T., et al., 2023b. CO₂ huff-n-puff combined with radial borehole fracturing to enhance oil recovery and store CO₂ in a shale oil reservoir. Geoenergy Sci. Eng., 212012 https://doi.org/10.1016/j.geoen.2023.212012.
- Dai, J., Zheng, Z., Wang, T., et al., 2023c. Productivity and cost comparison between radial-borehole fracturing and horizontal well fracturing in shale oil reservoir. In: SPE Gas & Oil Technology Showcase and Conference. https://doi.org/10.2118/ 214197-MS.
- Dai, J., Tian, K., Xue, Z., et al., 2023d. CO₂-Enhanced radial borehole development of shale oil: production simulation and parameter analysis. Process 12 (1), 116. https://doi.org/10.3390/pr12010116.
- Deng, H., Sheng, G., Zhao, H., et al., 2022. Integrated optimization of fracture parameters for subdivision cutting fractured horizontal wells in shale oil reservoirs. J. Petrol. Sci. Eng. 212, 110205. https://doi.org/10.1016/j.petrol.2022.110205.
- Dong, M., Shi, X., Ling, S., et al., 2019. Effect of dynamic pseudo threshold pressure gradient on well production performance in low-permeability and tight oil reservoirs. J. Petrol. Sci. Eng. 173, 69–76. https://doi.org/10.1016/ i.petrol.2018.09.096.
- Faisal, A., Bisdom, K., Zhumabek, B., et al., 2009. Injectivity and gravity segregation in WAG and SWAG enhanced oil recovery. In: SPE Annual Technical Conference and Exhibition. https://doi.org/10.2118/124197-MS.
- Gangi, A.F., 1978. Variation of whole and fractured porous rock permeability with confining pressure. Int. J. Rock Mech. Min. Sci. Geomech. Abstracts 5, 249–257. https://doi.org/10.1016/0148-9062(78)90957-9.
- Gao, Y., Zhao, M., Wang, J., et al., 2014. Performance and gas breakthrough during CO₂ immiscible flooding in ultra-low permeability reservoirs. Petrol. Explor. Dev. 41 (1), 88–95. https://doi.org/10.1016/S1876-3804(14)60010-0.
- Ghaderi, S.M., Clarkson, C.R., Chen, S., 2012a. Optimization of WAG process for coupled CO₂ EOR-storage in tight oil formations: an experimental Design approach. In: SPE Canada Unconventional Resources Conference. https:// doi.org/10.2118/161884-MS.
- Ghaderi, S.M., Clarkson, C.R., Chen, S., et al., 2012b. Evaluation of recovery performance of miscible displacement and WAG process in tight oil formations. In: SPE/EAGE European Unconventional Resources Conference and Exhibition. https://doi.org/10.2118/152084-MS.
- Guo, T., Qu, Z., Gong, D., et al., 2016. Numerical simulation of directional propagation of hydraulic fracture guided by vertical multi-radial boreholes. J. Nat. Gas Sci. Eng. 35, 175–188. https://doi.org/10.1016/j.jngse.2016.08.056.
- Guo, T., Liu, B., Qu, Z., et al., 2017. Study on initiation mechanisms of hydraulic fracture guided by vertical multi-radial boreholes. Rock Mech. Rock Eng. 50, 1767–1785. https://doi.org/10.1007/s00603-017-1205-3.
- Guo, Y., Liu, F., Qiu, J., et al., 2022. Microscopic transport and phase behaviors of CO₂ injection in heterogeneous formations using microfluidics. Energy 256, 124524. https://doi.org/10.1016/j.energy.2022.124524.
- Guo, Z., Tian, S., Liu, Q., et al., 2022. Experimental investigation on the breakdown pressure and fracture propagation of radial borehole fracturing. J. Petrol. Sci. Eng. 208, 109169. https://doi.org/10.1016/j.petrol.2021.109169.
- Hinderaker, L., Njaa, S., 2010. Utilization of associated petroleum gas (APG)—the

Norwegian experience. In: SPE Russian Petroleum Technology Conference. https://doi.org/10.2118/136316-MS.

- Höök, M., Davidsson, S., Johansson, S., et al., 2014. Decline and depletion rates of oil production: a comprehensive investigation. Phil. Trans. Math. Phys. Eng. Sci. 372 (2006), 20120448. https://doi.org/10.1098/rsta.2012.0448.
- Jia, B., Tsau, J.S., Barati, R., 2019a. Measurement of CO₂ diffusion coefficient in the oil-saturated porous media. J. Petrol. Sci. Eng. 181, 106189. https://doi.org/ 10.1016/j.petrol.2019.106189.
- Jia, B., Tsau, J.S., Barati, R., 2019b. A review of the current progress of CO₂ injection EOR and carbon storage in shale oil reservoirs. Fuel 236, 404–427. https:// doi.org/10.1016/i.fuel.2018.08.103.
- Jiang, J., Yang, J., 2018. Coupled fluid flow and geomechanics modeling of stress-sensitive production behavior in fractured shale gas reservoirs. Int. J. Rock Mech. Min. Sci. 101, 1–12. https://doi.org/10.1016/j.ijrmms.2017.11.003.
- Khan, M.Y., Mandal, A., 2020. Analytical model for gravity segregation in WAG displacement recovery of inclined stratified reservoirs. J. Petrol. Sci. Eng. 186, 106722. https://doi.org/10.1016/j.petrol.2019.106722.
- Khan, M.Y., Mandal, A., 2022a. Analytical model of incremental oil recovery as a function of WAG ratio and tapered WAG ratio benefits over uniform WAG ratio for heterogeneous reservoir. J. Petrol. Sci. Eng. 209, 109955. https://doi.org/ 10.1016/j.petrol.2021.109955.
- Khan, M.Y., Mandal, A., 2022b. The impact of permeability heterogeneity on wateralternating-gas displacement in highly stratified heterogeneous reservoirs. J. Pet. Explor. Prod. Technol. 12 (3), 871–897. https://doi.org/10.1007/s13202-021-01347-3.
- Khurshid, I., Afgan, I., 2021a. Geochemical investigation of CO₂ Injection in oil and gas reservoirs of Middle East to estimate the formation damage and related oil recovery. Energies. https://doi.org/10.3390/en14227676.
- Khurshid, I., Afgan, I., 2021b. Investigation of water composition on formation damage and related energy recovery from geothermal reservoirs: geochemical and geomechanics insights. Energies. https://doi.org/10.3390/en14217415.
- Khurshid, I., Afgan, I., 2022. Geochemical investigation of electrical conductivity and electrical double layer based wettability alteration during engineered water injection in carbonates. J. Petrol. Sci. Eng. 215, 110627. https://doi.org/10.1016/ j.petrol.2022.110627.
- Khurshid, I., Al-Shalabi, E.W., Afgan, I., et al., 2022a. New insights into surfactant adsorption estimation in carbonates under harsh conditions using surface complexation modeling. SPE Reservoir Eval. Eng. 25 (3), 397–413. https:// doi.org/10.2118/207912-PA.
- Khurshid, I., Al-Shalabi, E.W., Afgan, I., et al., 2022b. Geochemical modeling of engineered water injection in carbonates under harsh conditions: new insights with ionic adsorption. J. Energy Resour. Technol. 145 (2). https://doi.org/10.1115/ 14054956
- Lei, H., He, L., Li, R., et al., 2019. Effects of boundary layer and stress sensitivity on the performance of low-velocity and one-phase flow in a shale oil reservoir: experimental and numerical modeling approaches. J. Petrol. Sci. Eng. 180, 186–196. https://doi.org/10.1016/j.petrol.2019.05.025.
- Li, H., Zheng, S., Yang, D., 2013. Enhanced swelling effect and viscosity reduction of solvent(s)/CO₂/heavy-oil systems. SPE J. 18 (4), 695–707. https://doi.org/10.2118/150168_PA
- Li, J., Huang, Z., Li, G., et al., 2022. Field test of radial jet drilling technology in a surface formation. J. Petrol. Sci. Eng. 218, 110928. https://doi.org/10.1016/ i.petrol.2022.110928.
- Li, L., Su, Y., Hao, Y., et al., 2019. A comparative study of CO₂ and N₂ huff-n-puff EOR performance in shale oil production. J. Petrol. Sci. Eng. 181, 106174. https://doi.org/10.1016/j.petrol.2019.06.038.
- Liu, B., Wang, C., Zhang, J., et al., 2017. Displacement mechanism of oil in shale inorganic nanopores by supercritical carbon dioxide from molecular dynamics simulations. Energy & Fuels 31 (1), 738–746. https://doi.org/10.1021/ acs.energyfuels.6b02377.
- Liu, B., Yang, Y., Li, J., et al., 2020. Stress sensitivity of tight reservoirs and its effect on oil saturation: a case study of Lower Cretaceous tight clastic reservoirs in the Hailar Basin, Northeast China. J. Petrol. Sci. Eng. 184, 106484. https://doi.org/ 10.1016/j.petrol.2019.106484.
- Liu, Q., Tian, S., Li, G., et al., 2018. An analytical model for fracture initiation from radial lateral borehole. J. Petrol. Sci. Eng. 164, 206–218. https://doi.org/10.1016/ i.petrol.2018.01.056
- Massarweh, O., Abushaikha, A.S., 2022. A review of recent developments in CO₂ mobility control in enhanced oil recovery. Petroleum 8 (3), 291–317. https://doi.org/10.1016/j.petlm.2021.05.002.
- Maut, P.P., Jain, D., Mohan, R., et al., 2017. Production enhancement in mature fields of Assam Arakan basin by radial jet drilling-a case study. In: SPE Symposium: Production Enhancement and Cost Optimisation. https://doi.org/10.2118/189243-MS.
- Nwachukwu, A., Jeong, H., Sun, A., et al., 2018. Machine learning-based optimization of well locations and WAG parameters under geologic uncertainty. In: SPE Improved Oil Recovery Conference. https://doi.org/10.2118/190239-MS.
- Orangi, A., Nagarajan, N.R., Honarpour, M.M., et al., 2011. Unconventional shale oil and gas-condensate reservoir production, impact of rock, fluid, and hydraulic fractures. In: SPE Hydraulic Fracturing Technology Conference and Exhibition. https://doi.org/10.2118/140536-MS.
- Qi, P., Chen, Y., Temple, P., et al., 2024. Leveraging machine learning to optimize CO₂-WAG flooding for enhanced oil recovery and carbon storage. In: the Offshore Technology Conference. https://doi.org/10.4043/35456-MS.
- Qu, J., Tang, Z., Lei, G., et al., 2024. A novel threshold pressure gradient model and its

- influence on production simulation for shale oil reservoirs. Energy & Fuels. https://doi.org/10.1021/acs.energyfuels.4c00320.
- Ragab, A.M., Kamel, A.M., 2013. Radial drilling technique for improving well productivity in Petrobel-Egypt. In: North Africa Technical Conference and Exhibition. https://doi.org/10.2118/164773-MS.
- Ren, D., Wang, X., Kou, Z., et al., 2023. Feasibility evaluation of CO₂ EOR and storage in tight oil reservoirs: a demonstration project in the Ordos Basin. Fuel 331, 125652. https://doi.org/10.1016/j.fuel.2022.125652.
- Roe, P.L., 1986. Characteristic-based schemes for the Euler equations. Annu. Rev. Fluid Mech. 18 (1), 337–365. https://doi.org/10.1146/annurev.fl.18.010186.002005.
- Rui, Z.H., Deng, H.Y., Hu, T., et al., 2025. Coupling mechanism analysis of CO₂ non-Darcy flow in multi-scale reservoirs: a case study of the life-cycle process of fracturing-development in shale oil reservoirs. Pet. Sci. 22 (3), 1171–1199. https://doi.org/10.1016/j.petsci.2024.12.018.
- Shen, Z., Sheng, J.J., 2018. Experimental and numerical study of permeability reduction caused by asphaltene precipitation and deposition during CO₂ huff and puff injection in Eagle Ford shale. Fuel 211, 432–445. https://doi.org/10.1016/j.fuel.2017.09.047.
- Sheng, J.J., 2017. Optimization of huff-n-puff gas injection in shale oil reservoirs. Petroleum 3 (4), 431–437. https://doi.org/10.1016/j.petlm.2017.03.004.
- Skauge, A., Stensen, J.Å., 2003. Review of WAG field experience. In: Oil Recovery—2003, 1st International Conference and Exhibition, Modern Challenges in Oil Recovery. https://doi.org/10.2118/39883-MS.
- Stalkup, F.I., 1978. Carbon dioxide miscible flooding: past, present, and outlook for the future. J. Petrol. Technol. 30 (8), 1102–1112. https://doi.org/10.2118/7042-
- Suliman, B., Meek, R., Hull, R., et al., 2013. Variable stimulated reservoir volume (SRV) simulation: Eagle ford shale case study. In: SPE Unconventional Resources Conference-USA. https://doi.org/10.1190/urtec2013-057.
- Sun, X., Liu, J., Dai, X., et al., 2021. On the application of surfactant and water alternating gas (SAG/WAG) injection to improve oil recovery in tight reservoirs. Energy Rep. 7, 2452–2459. https://doi.org/10.1016/j.egyr.2021.04.034.
- Tian, Y., Xiong, Y., Wang, L., et al., 2019. A compositional model for gas injection IOR/ EOR in tight oil reservoirs under coupled nanopore confinement and geomechanics effects. J. Nat. Gas Sci. Eng. 71, 102973. https://doi.org/10.1016/ j.jngse.2019.102973.
- Tovar, F.D., Barrufet, M.A., Schechter, D.S., 2021. Enhanced oil recovery in the wolfcamp shale by carbon dioxide or nitrogen injection: an experimental investigation. SPE J. 26 (1), 515–537. https://doi.org/10.2118/204230-PA.
- Wan, T., Sheng, J.J., 2015. Evaluation of the EOR potential in hydraulically fractured shale oil reservoirs by cyclic gas injection. Petrol. Sci. Technol. 33 (7), 812–818. https://doi.org/10.1190/urtec2013-187.
- Wang, G., Pickup, G., Sorbie, K., et al., 2020. Numerical study of CO₂ injection and the role of viscous crossflow in near-miscible CO₂-WAG. J. Nat. Gas Sci. Eng. 74, 103112. https://doi.org/10.1016/j.jngse.2019.103112.
- Wang, H., Su, Y., Wang, W., et al., 2022. CO₂-oil diffusion, adsorption and miscible flow in nanoporous media from pore-scale perspectives. Chem. Eng. J. 450, 137957. https://doi.org/10.1016/j.cej.2022.137957.
- Wang, H., Kou, Z., Ji, Z., et al., 2023. Investigation of enhanced CO₂ storage in deep saline aquifers by WAG and brine extraction in the Minnelusa sandstone, Wyoming. Energy 265, 126379. https://doi.org/10.1016/j.energy.2022.126379.
- Wang, J., Luo, H., Liu, H., et al., 2017. An integrative model to simulate gas transport and production coupled with gas adsorption, non-Darcy flow, surface diffusion, and stress dependence in organic-shale reservoirs. SPE J. 22 (1), 244–264. https://doi.org/10.2118/174996-PA.
- Wang, X., Sheng, J.J., 2017. Effect of low-velocity non-Darcy flow on well production performance in shale and tight oil reservoirs. Fuel 190, 41–46. https://doi.org/ 10.1016/j.fuel.2016.11.040.
- Wu, D., Brantson, E.T., Ju, B., 2021. Numerical simulation of water alternating gas flooding (WAG) using CO₂ for high-salt argillaceous dolomite reservoir considering the impact of stress sensitivity and threshold pressure gradient. Acta Geophys. 69 (4), 1349–1365. https://doi.org/10.1007/s11600-021-00601-w.
- Wu, Z., Cui, C., Lv, G., et al., 2019. A multi-linear transient pressure model for multistage fractured horizontal well in tight oil reservoirs with considering threshold pressure gradient and stress sensitivity. J. Petrol. Sci. Eng. 172, 839–854. https://doi.org/10.1016/j.petrol.2018.08.078.
- Xia, D., Yang, Z., Gao, T., et al., 2021. Characteristics of micro-and nano-pores in shale oil reservoirs. J. Petrol. Explor. Prod. 11, 157–169. https://doi.org/10.1007/ s13202-020-01012-1.
- Xiao, W., Li, T., Li, M., et al., 2016. Evaluation of the stress sensitivity in tight reservoirs. Petrol. Explor. Dev. 43 (1), 115–123. https://doi.org/10.1016/S1876-3804(16)30013-1.
- Yang, D., Wang, W., Li, K., et al., 2019. Experimental investigation on the stress sensitivity of permeability in naturally fractured shale. Environ. Earth Sci. 78, 1–10. https://doi.org/10.1016/j.fuel.2019.116078.
- Yang, R.Y., Li, G.S., Qin, X.Z., et al., 2022. Productivity enhancement in multilayered coalbed methane reservoirs by radial borehole fracturing. Pet. Sci. 19 (6), 2844–2866. https://doi.org/10.1016/j.petsci.2022.06.019.
- Yang, S., Wu, K., Xu, J., et al., 2019. Roles of multicomponent adsorption and geomechanics in the development of an Eagle Ford shale condensate reservoir. Fuel 242, 710–718. https://doi.org/10.1016/j.fuel.2019.01.016.
- Yao, Y., Ge, J., 2011. Characteristics of non-Darcy flow in low-permeability reservoirs. Pet. Sci. 8, 55–62. https://doi.org/10.1007/s12182-011-0115-3.
- Yu, W., Zhang, Y., Varavei, A., et al., 2019. Compositional simulation of CO₂ huff'n'puff in Eagle Ford tight oil reservoirs with CO₂ molecular diffusion,

- nanopore confinement, and complex natural fractures. SPE Reservoir Eval. Eng.
- 22 (2), 492–508. https://doi.org/10.2118/190325-MS.
 Zeng, J., Cheng, S., Kong, X., et al., 2010. Non-Darcy flow in oil accumulation (oil displacing water) and relative permeability and oil saturation characteristics of low-permeability sandstones. Pet. Sci. 7, 20–30. https://doi.org/10.1007/s12182-010-0003-2.
- Zhang, Y., Lu, R., Forouzanfar, F., et al., 2017. Well placement and control optimization for WAG/SAG processes using ensemble-based method. Comput. Chem. Eng. 101, 193-209. https://doi.org/10.1016/j.compchemeng.2017.02.020.
- Zhao, X., Chen, Z., Wang, B., et al., 2023. A multi-medium and multi-mechanism model for CO2 injection and storage in fractured shale gas reservoirs. Fuel
- 345, 128167. https://doi.org/10.1016/j.fuel.2023.128167. Zhao, Y., Zhang, Y., Lei, X., et al., 2020. CO_2 flooding enhanced oil recovery evaluated using magnetic resonance imaging technique. Energy 203, 117878. https:// doi.org/10.1016/j.energy.2020.117878.
- Zhou, X., Yuan, Q., Zhang, Y., et al., 2019. Performance evaluation of CO₂ flooding process in tight oil reservoir via experimental and numerical simulation studies. Fuel 236, 730–746. https://doi.org/10.1016/j.fuel.2018.09.035.
- Zhu, C., Li, Y., Zhao, Q., et al., 2018. Experimental study and simulation of CO₂ transfer processes in shale oil reservoir. Int. J. Coal Geol. 191, 24–36. https:// doi.org/10.1016/j.coal.2018.03.002.